Space Science Reviews (2026) 222:26
https://doi.org/10.1007/s11214-026-01274-x

SPECIAL COMMUNICATION

The High-Energy Particle Detector on Board the CSES-02 Satellite

Simona Bartocci · Roberto Battiston · Stefania Beolè · Franco Benotto · Piero Cipollone · Silvia Coli et al. ***[full author details at the end of the article]***

Received: 6 September 2025 / Accepted: 2 February 2026

Abstract
The China Seismo-Electromagnetic Satellite (CSES) mission is a joint China-Italy initiative focused on investigating Earth's geophysical environment through non-imaging remote sensing from space. Its primary objective is to establish a constellation of satellites capable of continuously monitoring global electromagnetic fields, particle fluxes, and plasma parameters within the iono-magnetospheric system. Goals of this space program are the investigation of possible lithosphere-atmosphere-ionosphere-magnetosphere coupling mechanisms and their role in inducing perturbations in the upper ionosphere and the lower boundary of the radiation belts. Additionally, CSES contributes to space weather studies, including investigations of the magnetosphere, heliosphere, and galactic cosmic rays. Each satellite in the constellation carries multiple instruments to measure charged particles, electromagnetic fields, and plasma properties. CSES-01, launched in February 2018, remains operational. The second satellite, CSES-02, was launched on June 14, 2025, marking the transition to a multi-point observation capability. Italy contributed the High-Energy Particle Detector to both missions—HEPD-01 for CSES-01 and the upgraded HEPD-02 for CSES-02. These detectors are designed for precise measurements of electrons, protons, light nuclei, and transient gamma rays in the multi-MeV range. HEPD-02 significantly enhances energy resolution and extends the detection range when combined with the lower-energy instruments aboard CSES-02, enabling continuous coverage from 100 keV to 200 MeV. This article presents the scientific goals of the CSES program, with a focus on the role of HEPD-02 in energetic particle studies, both as a standalone detector and in synergy with the mission's multi-instrument, multi-satellite framework.

Keywords CSES-02 mission · High-Energy Particle Detector HEPD · Space weather · Radiation belts · Cosmic rays · Lithosphere-ionosphere coupling

1 Introduction

The near-Earth environment (NEE) surrounds the lithosphere, includes the atmosphere, the ionosphere and extends into the heliospheric deep space with the magnetosphere (see Fig. 1). The NEE is a highly dynamic region, hosting numerous phenomena distinctive to its various layers and their couplings, under the influence of the solar forcing. The study of the NEE greatly benefits from in-situ measurements provided by satellite observatories. Satellites operating in polar low Earth orbit (LEO) provide a unique observational point for studying

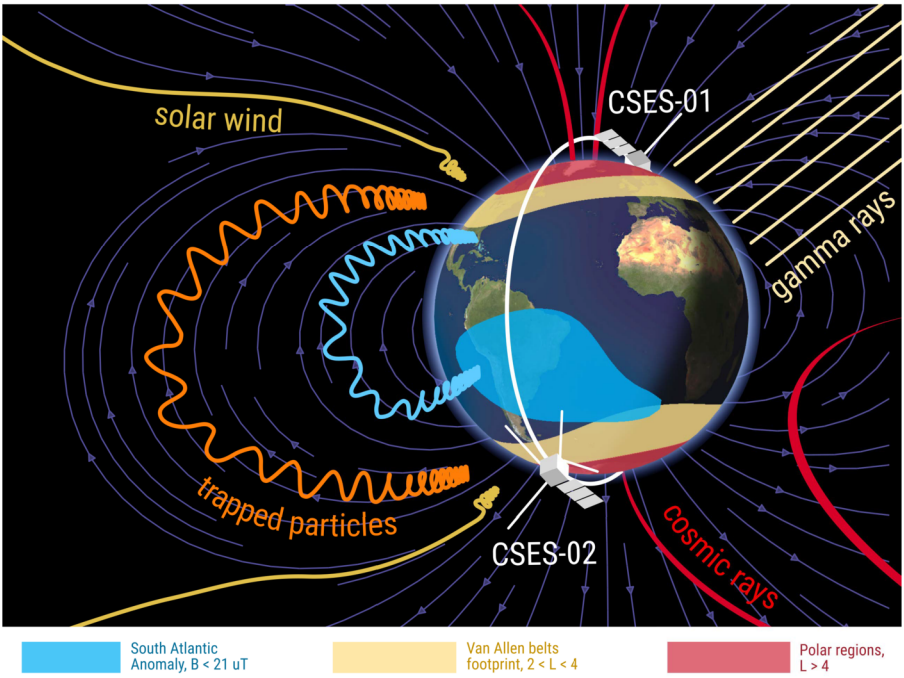

Fig. 1 Charged particle and gamma-ray observation domains of CSES-01 and CSES-02. The illustration highlights the satellites' sensitivity to trapped particles, cosmic rays, gamma rays, and their trajectories relative to major geophysical and magnetospheric features such as the South Atlantic Anomaly, Van Allen belts, and polar regions

particles, plasma and electromagnetic field interactions: at latitudes below $\sim 70°$ they are sensitive to trapped particles and ionospheric phenomena while at higher latitudes they are in direct contact with the heliosphere and the flux of Low Energy Cosmic Rays (Gabici 2022). During the last 30 years, the NEE has been studied systematically, using specialized probes focused on specific measurements. Various missions studied energetic particles in NEE, including the Solar Anomalous and Magnetospheric Particle Explorer (SAMPEX, 1992-2012, (Baker et al. 1993)), the Van Allen Probes (2012-2019, (Spence et al. 2013)) and the Exploration of energization and Radiation in Geospace (ERG Arase, 2016-present, (Miyoshi et al. 2018)). The Earth's magnetic field has been studied by the Cluster constellation (2000-present, (Escoubet et al. 2001)), Swarm (2013-present, (Macmillan and Olsen 2013)) and the Challenging Minisatellite Payload (CHAMP, 2000-2010, (Reigber et al. 2003)). The ionosphere is being regularly monitored by missions such as Time History of Events and Macroscale Interactions during Substorms (THEMIS, 2007-present, (Sibeck and Angelopoulos 2008)), Defense Meteorological Satellite Program (DMSP, 1962-present, (Force 1962)) and Thermosphere, Ionosphere, Mesosphere Energetics and Dynamics (TIMED, 2001-present, (Kusnierkiewicz 2003)). The magnetosphere and near-Earth space weather phenomena are studied by missions like Wind (1994-present, (Ogilvie et al. 1995)), the Advanced Composition Explorer (ACE, 1997-present, (Stone et al. 1998)), THEMIS, and the Magnetospheric MultiScale (MMS) constellation (2015-present, (Burch et al. 2016)).

These missions have improved the understanding of the various NEE layers, paving the way for studying their coupling mechanisms. However the NEE can be seen as a giant

volume sensitive to terrestrial, solar and astrophysical phenomena. Following the pioneering experience of DEMETER (Detection of Electro-Magnetic Emissions Transmitted from Earthquake Regions) mission (Parrot et al. 2006a; Berthelier et al. 2006) (2004-2010), the CSES constellation has been developed to exploit the potential of this concept, with specific focus on the monitoring of the Earth geophysical hazards from space.

The launch of CSES-01 took place in February 2018 (Shen et al. 2018; Picozza et al. 2019) while CSES-02 was successfully launched on June 14, 2025.

In this paper we are reviewing the CSES constellation science case, focusing on the contribution of the High-Energy Particle Detector (HEPD-02) payload developed by the Italian CSES-Limadou Collaboration.

This article is structured as follows: Sect. 2 provides an overview of the general scientific objectives and the rationale of the CSES constellation. Section 3 delves into the specific scientific aspects related to HEPD-02 aboard CSES-02. Section 4 offers a detailed description of the HEPD-02 instrument and its expected in-flight performance. Finally, Sect. 5 presents our conclusions.

2 Scientific Objectives and Rationale of the CSES Constellation

The CSES (China Seismo-Electromagnetic Satellite) constellation builds on the legacy of DEMETER, the first satellite (2004–2010) specifically designed to investigate non-imaging electromagnetic emissions from geophysical, tropospheric, magnetospheric, and solar phenomena (Parrot 2002). While DEMETER did not provide conclusive evidence for seismic precursors, it made important discoveries (e.g. Parrot et al. 2006b; Molchanov et al. 2006; Sarkar et al. 2007; Němek et al. 2008; Akhoondzadeh et al. 2010; Harrison et al. 2010), and laid the groundwork for the CSES program.

Launched in 2018, CSES-01 continues to operate beyond its expected five-year lifespan. CSES-02 features a similar but technologically enhanced payload and is designed for a mission lasting at least six years. Both satellites share a Sun-synchronous orbit at $\sim$500 km altitude and 98° inclination, with CSES-02 positioned 180° apart. This configuration enables correlated observations and reduces the revisit time from five to 2.5 days, improving the temporal coverage.

The CSES-02 payload suite includes (see Table 1 for details): two particle detectors complementary in energy coverage (HEPD-02 and MEED), high-precision and search-coil magnetometers (HPM and SCM), an electric field detector (EFD-02) (Diego et al. 2025), a Coherent Population Trap (CPT), Global Navigation Satellite System (GNSS) Occultation Receiver (GOR), Tri-Band Beacon (TBB), Langmuir Probe (LP), Ionospheric Photometer (IP), and Plasma Analyzer Package (PAP).

The mission's scientific goals cover a wide range of geophysical, atmospheric, magnetospheric, and astrophysical phenomena, aiming at (i) monitoring and model the Earth's ionosphere and magnetosphere dynamics; (ii) investigating co-seismic and possible precursor phenomena; (iii) studying wave-particle interactions and radiation belt dynamics; (iv) detecting charged particles and transient gamma events.

2.1 Geophysical Hazards and Earthquake-Related Phenomena

The CSES constellation provides advanced capabilities for detecting possible electromagnetic and plasma perturbations linked to fast geophysical phenomena such as earthquakes, volcanic eruptions, and tsunamis. Co-seismic phenomena, including acoustic-gravity waves

Table 1 Description of physics goals and physical observables for the payloads on board the CSES-02 satellite. Details about specific physical channels are given for each payload

Type of Physics	Payload name	Observables
Particles and nuclei	High-Energy Particle Detector (HEPD-02)	Electrons: 3 to 100 MeV; Protons and nuclei: 30 to 200 MeV/n;
	Medium Energetic Electron Detector (MEED)	Electrons: 25 keV to 3.2 MeV
Electromagnetic field	Electric Field Detector (EFD-02)	Electric field: DC to 3.5 MHz
	High Precision Magnetometer (HPM)	Magnetic field: DC to 15 Hz
	Search Coil Magnetometer (SCM)	Magnetic field: 10 Hz to 20 kHz;
	Coherent Population Trap (CPT)	Magnetic Field: DC to 15 Hz
In situ plasma	Plasma Analyzer Package (PAP)	N_e: $5 \cdot 10^2$ to $1 \cdot 10^7$ cm^{-3}; Composition: H+, He+, O+
	Langmuir Probe (LP)	T_e: 500 to 10,000 K
Plasma profile construction	GNSS Occultation Receiver (GOR)	TEC by GNSS Occultation Signal
	Tri-Band Beacon (TBB)	TEC by transmit VH/U/L signal
	Ionospheric Photometer (IP)	O_2 at 135.6 nm and N_2LBH airglow

(AGWs) generated by large-scale ground motion, have been observed to couple into the ionosphere (Kaladze et al. 2008). Based on CSES-01 data, some members of the CSES-Limadou Collaboration developed and tested the Magnetosphere-Ionosphere-Lithosphere coupling (MILC) model, which calculates disturbances observed at satellite altitude (Carbone et al. 2021).

While models for earthquake precursors—such as the Lithosphere-Atmosphere-Ionosphere coupling (LAIC) framework—exist, they remain largely qualitative (Pulinets 1998). The enhanced sensitivity, spatial resolution, and coverage of the CSES-02 satellite will provide the best opportunity yet to test these models rigorously and explore precursor signatures with unprecedented accuracy.

2.2 Ionosphere Dynamics

The ionosphere, ranging from 60 km to ∼1000 km in altitude, is a complex and variable plasma environment influenced by solar radiation, geomagnetic storms, and atmospheric dynamics (e.g. Tsurutani et al. 2009; Liu et al. 2011; Titheridge 1995). Understanding its variability is crucial for space weather modeling, GPS and communication reliability, and ionospheric physics (e.g. Rishbeth 1988; Kintner et al. 2007).

CSES-01 has already enabled the characterization of ionospheric disturbances driven by both space weather and atmospheric-origin phenomena (Zhao et al. 2019; Yang et al. 2020; Yan et al. 2020; Zhima et al. 2020, 2021; Astafyeva et al. 2022; Papini et al. 2023). The CSES-02 mission aims at enhancing this capability and improving sensitivity to potential seismo-associated signals.

2.3 Wave-Particle Interactions

Wave-particle interactions in the magnetosphere mediate key processes such as particle acceleration, wave growth, and radiation belt evolution. CSES data support the study of: (i) whistler-mode chorus waves (Bortnik and Thorne 2007); (ii) Electromagnetic Ion Cyclotron (EMIC) waves (Thorne 2010; Baker 2021); (iii) Alfvén waves linked to auroral activity (Rae et al. 2005).

These processes underpin phenomena from auroral displays to geomagnetic storms and contribute to space weather forecasting and mitigation strategies.

2.4 Charged Particles and Transient Astrophysics

Figure 1 illustrates the regions of space and types of particle phenomena observable by the CSES-01 and CSES-02 detectors, including cosmic rays, trapped particles, and gamma transients, as well as key geophysical features such as the South Atlantic Anomaly and the Van Allen belts. By means of its particle detectors, the CSES constellation will provide insights into solar modulation, magnetospheric particle dynamics, and transient events, complementing ground-based and other space-borne missions. Further discussion of these topics is presented in the next section.

3 HEPD-02 on the CSES-02 Mission

HEPD-02 is a compact, lightweight, and low-power consumption detector optimized for observing protons, electrons and light nuclei across a wide range of energies. During the satellite mission, the instrument is constantly oriented towards the zenith, ensuring an unobstructed view for particle detection.

The first version of this detector, HEPD-01, is still flying on CSES-01 yet not operational since July 2022 due to a permanent failure, likely caused by radiation effects, which rendered the payload unrecoverable despite several attempts to restore its functionality. A general overview of HEPD-01 detector is given in Ambrosi et al. (2020), Picozza et al. (2019), Sotgiu et al. (2020), Ambrosi et al. (2021).

A key improvement present in the CSES-02 mission, as compared to the predecessor, is that the satellite enables continuous data collection throughout the entire orbit. This will allow HEPD-02 to conduct extended observations of polar and near-polar regions, where cosmic rays of galactic origin are most dominant.

Moreover, HEPD-02 features several upgrades as compared to HEPD-01, including a more precise tracking device that improves the reconstruction of particle arrival directions. The calorimetric section of the instrument also presents increased energy resolution and sensitivity range.

As a result, the new detector will not only extend the observations initiated by HEPD-01 but will also open new opportunities for exploring cosmic-ray and solar physics.

A complete description of HEPD-02's functionality and performance is provided in Sect. 4. The following paragraphs focus on a detailed overview of the HEPD-02 scientific objectives.

3.1 Galactic Cosmic Radiation and Solar Modulation

The fraction of time available to CSES-02 to collect data above the geomagnetic cut-off increases 3-to-35 times according to the rigidity (see Fig. 2), enabling the full exploitation of the HEPD-02 sensitivity range to detect Galactic Cosmic Rays.

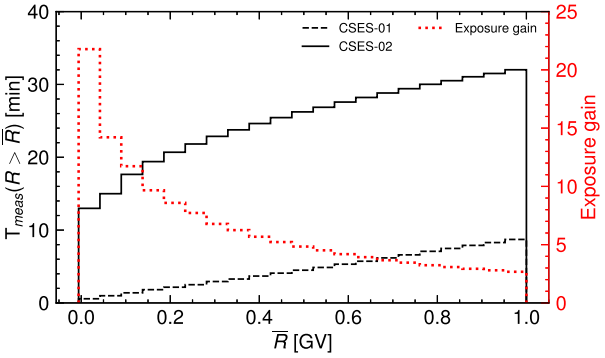

Fig. 2 Average time per orbit during which galactic particles are observed above a given cutoff rigidity $\bar{R}$. A comparison between CSES-02 (black solid line) and CSES-01 (black dashed line) highlights the increased sensitivity to low energetic, galactic particles for the former. The red dotted line highlights the exposure gain between CSES-02 and CSES-01 above a given $\bar{R}$

Electrons down to 3 MeV and protons down to 30 MeV are usually referred to as low-energy cosmic rays (LECRs) and play a crucial role in the physics and the chemistry of the galactic interstellar medium Gabici (2022).

The Voyager 1 and 2 probes Stone et al. (2013, 2019) crossed the heliopause and entered interstellar space in 2013 and 2018, respectively, enabling *in situ* measurements of the Local Interstellar Spectrum of LECRs. They directly detected them outside the heliosphere, down to energies as low as a few MeV. The data collected by the Voyager probes have offered unprecedented insights into LECRs, overcoming previous observational challenges posed by solar modulation.

The most precise data ever gathered about LECRs up to 10 GeV/nucleon are due to the Payload for Antimatter Matter Exploration and Light Nuclei Astrophysics (PAMELA) Picozza et al. (2007) and Alpha Magnetic Spectrometer (AMS) Aguilar et al. (2021) missions. They provided both high-sensitivity measurements of the local spectra of various galactic cosmic-ray species, including protons and helium nuclei, and crucial information to constrain the properties of the local interstellar spectrum of LECRs.

The High-Energy Particle Detectors onboard the CSES satellites offer observational capabilities that complement those of the Cosmic Ray Isotope Spectrometer (CRIS) on board the Advanced Composition Explorer (ACE) and the Solar and Galactic Proton Sensor (SGPS) units of the Geostationary Operational Environmental Satellite (GOES). From 2018 to 2022, HEPD-01 measured the cosmic-ray proton spectrum (Bartocci et al. 2020) in the 40 to 250 MeV range. HEPD-02, designed with improved sensitivity, enhances our understanding of LECRs transport properties and interactions with the interstellar medium.

Galactic cosmic-ray particles reaching the Earth are affected by the solar wind, a continuous flow of plasma originating from the solar corona, extending beyond the limits of the solar system and traveling at supersonic (∼350 km/s) speeds (Bruno and Carbone 2013). The Sun's magnetic field is coupled to the solar wind plasma, which propagates throughout interplanetary space and forms the interplanetary magnetic field.

As well documented, solar activity varies with time, rising from a minimum to a maximum value and then returning to the minimum (solar cycle), with a ∼11 years periodicity (Usoskin 2023). This can be seen in Fig. 3, where the sunspot number recorded since 2012 (black markers) is used as a valid proxy for the evolution of the Sun's activity (more sunspots are expected during the maximum phases). Red and blue curves indicate the expected average number of sunspots in the period 2025–2032 — during the foreseen CSES-02 mission span — and its low and high-range values, respectively.

HEPD-02 will investigate the peak phase of solar cycle 25 and its descent towards the minimum setting the start of solar cycle 26 and beyond, allowing to compare the result-

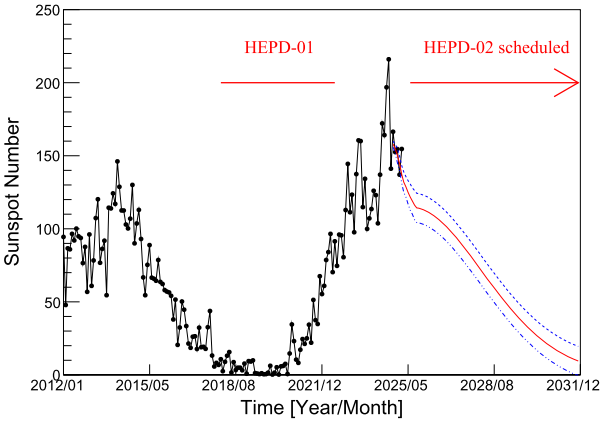

Fig. 3 Sunspot number as a function of time (black points) along with a prediction of the same quantity for the next ∼6 years (red curve is the average while blue curves represent low-range and high-range values). The plot highlights the different phases of solar cycle that HEPD-02 will monitor (descent towards the minimum) with respect to HEPD-01 (rise to the maximum). Data extracted from NOAA-SWPC (2025)

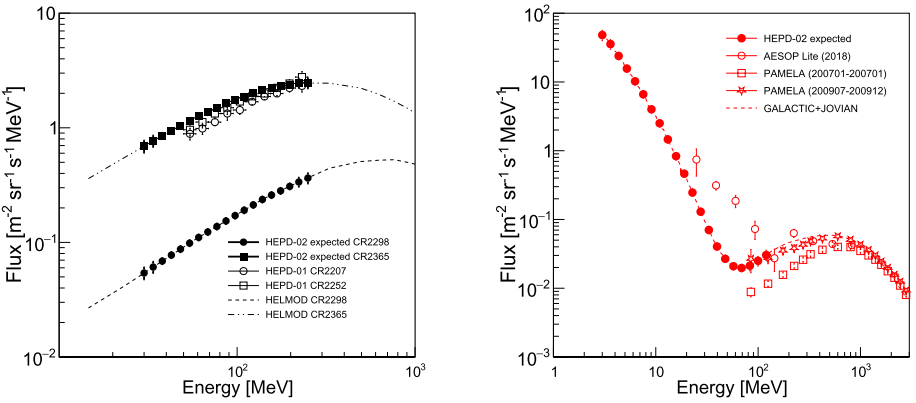

Fig. 4 Shown are the expected differential energy spectra for galactic protons (black markers in the left panel, averaged over Carrington Rotations CR2298 and CR2365) and galactic electrons (red markers in the right panel, integrated over the period June 2025–June 2026). For context, experimental results from HEPD-01 (protons), AESOP-Lite, PAMELA 2007 and PAMELA 2009 (all for electrons) are overlaid in both panels. The corresponding theoretical models — HELMOD for protons averaged over CR2298 and CR2365 and the one from Strauss et al. (see text) for electrons — are also provided for reference

ing observations on solar modulation effects with those collected by HEPD-01 during the previous cycle's minimum phase (Martucci et al. 2023a). Furthermore, given the expected operational lifespan of over six years, HEPD-02 could also explore the impact of the solar magnetic field polarity reversal — from the A^+ configuration of cycle 25 to the A^- configuration of cycle 26 — expected around 2031, providing valuable insights into low-energy particle behavior during this transition.

The expected differential energy spectra of protons and electrons are displayed in Fig. 4, left and right panels, respectively: protons below a few hundreds MeV are expected to be heavily affected by the modulating power of the Sun, contributing in a change in fluxes of about 1 order of magnitude from 2025 (black circles) to 2031 (black squares). These estimations have been performed over a Carrington Rotation (CR) basis.[1] Furthermore, two

[1]The standardized measure of the Sun's rotation, with a conventionally fixed period of 27.2753 days.

proton spectra obtained by HEPD-01 between 2018 and 2022 are superimposed as a reference (Martucci et al. 2023a). Galactic proton models obtained through HELMOD (Heliospheric Modulation) routines (Boschini et al. 2022) and integrated over the same time periods as the aforementioned estimated proton spectra. Conversely, small effects related to the Sun's activity are expected for leptons (e^-, e^+) below ∼30 MeV, as shown in the right panel of Fig. 4. However, these energy ranges are still poorly known, since most observations come from balloon-borne experiments carried out in the 70s and the 80s (Webber et al. 1973; Evenson and Meyer 1983). Also, the role of Jovian electrons at tens of MeV is still under study. Jupiter is a well-established point source of energetic electrons, and these particles can travel along interplanetary magnetic field lines to 1 AU under favorable connection conditions. Observations at Earth's orbit therefore offer an opportunity to investigate their propagation, modulation, and the influence of heliospheric structures on their transport (Moses et al. 1987; Chenette et al. 1977). In the same panel of Fig. 4, the all-electron ($e^- + e^+$) galactic flux expected to be detected by HEPD-02 is reported together with the all-electron spectrum from the newer balloon-borne mission Anti-Electron Sub-Orbital Payload (AESOP) Lite (Mechbal et al. 2020). PAMELA galactic e^- spectra recorded in 2007 and 2009 are also reported as a comparison, while the most advanced galactic+Jovian model (Strauss et al. 2011) is drawn as a reference. Differences in the spectra are expected due to the solar-cycle polarities corresponding to the data-taking periods of PAMELA (cycle 23), AESOP-Lite (cycle 24), and HEPD-02 (cycle 25).

Modulation of light nuclei with $Z > 1$, on the other hand, is a very much unexplored topic; like for electrons, most of the data at MeV energies can be traced back to balloon-borne missions and to the ACE spacecraft (Zhu et al. 2018). Furthermore, precision measurements of such nuclei are being carried out mainly by AMS-02 at much higher energies, see for example Aguilar et al. (2016, 2018b). Even if the term "modulation" usually refers to the long-term change in cosmic-ray flux, numerous small-scale variations have been identified as well, like the 13.5 and 27-day periodicities mentioned in Aguilar et al. (2018a), Siruk et al. (2024), Modzelewska et al. (2020), Kotzé (2023).

Finally, the capability of HEPD-02 to access the MeV-energy range allows it to shed light on less-known populations such as the Anomalous Cosmic Rays (ACRs), which are thought to originate from interstellar neutral atoms that become ionized and subsequently accelerated at the heliospheric termination shock, exhibiting distinct energy spectra and composition compared to galactic cosmic rays (Giacalone et al. 2022).

3.2 Solar Energetic Particle Events and Forbush Decreases

Solar energetic particles (SEPs) are high-energy charged particles (electrons, protons, and heavier ions) originating from the solar atmosphere, reaching energies up to GeV in extreme cases. They are typically produced by solar flares and coronal mass ejections (CMEs), then accelerated and transported through interplanetary space by the solar wind's magnetic field (Leer et al. 1982). SEPs are not only a scientific challenge due to their unpredictable nature (e.g. Huttunen-Heikinmaa et al. 2005; Mewaldt et al. 2005; Bruno et al. 2018), but also a recognized hazard to spacecraft, high-altitude aircraft, astronauts, and flight crews. Studying these effects is a key part of modern Space Weather research (e.g. Jackman et al. 2005; Damiani et al. 2008; Berrilli et al. 2014). During the solar cycle's maximum phase, powerful flares become more frequent, increasing the likelihood of intense SEP events exceeding hundreds of MeV (Aschwanden 2012). The CSES-01 heritage in Space Weather studies includes a range of results covering particles and other observables, as reported in Palma et al. (2021b), Piersanti et al. (2022), Bartocci et al. (2024a). Among its key achievements,

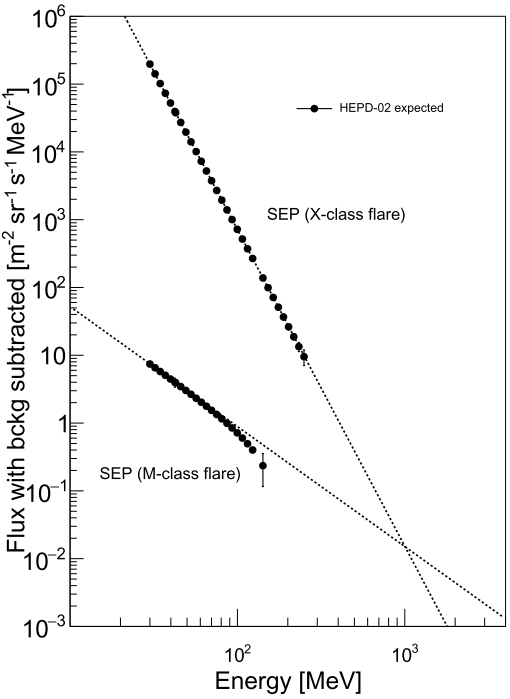

Fig. 5 Examples of differential proton spectra during two generic SEPs generated by M and X-class solar flares (dotted lines). Black markers represent the expected HEPD-02 capabilities in purely solar proton measurements (i.e. with quiet GCR background removed)

HEPD-01 successfully captured valuable data from the October 28, 2021 Ground Level Enhancement (GLE), providing insights into both the proton spectrum and the time of arrival for energies up to a few hundred MeV (Martucci et al. 2023b). Additionally, HEPD-01 reported similar observations for a series of medium SEP events in 2022 (Bartocci et al. 2024a).

HEPD-02 will start collecting data right around the start of the maximum phase of the current solar cycle allowing an in-depth investigation of medium-to-strong SEPs — common during such phase. Figure 5 shows examples of differential proton spectra during two generic SEPs generated by M and X-class solar flares (dashed lines). Black markers represent the expected HEPD-02 sensitivity after subtracting the Sun-quiet background flux from data including the SEP contribution. This sensitivity has been estimated with dedicated simulations (Bartocci et al. 2026b) and validated using data from HEPD-01, since the many aspects of the design philosophy for both detectors is basically the same. As can be seen, HEPD-02 is sensitive up to hundreds of MeV, making it suitable to evaluate, among other characteristics, the energetic extension of the solar injection.

SEPs are not the only Sun-related transients observable from Earth. CMEs — and their interplanetary counterparts, interplanetary CMEs (ICMEs) — can significantly influence the near-Earth environment, alongside other solar structures such as stream interaction regions (SIRs) and corotating interaction regions (CIRs) (e.g. Rouillard et al. 2011; Zhang et al. 2021). ICMEs are a well-known cause of Forbush decreases — sudden drops in cosmic-ray intensity — driven by strong disturbances in the geomagnetic field. The extent of this decrease, and its dependence on particle species, charge, mass, and energy, remains an open area of research (e.g. Lockwood 1971; Cane 2000; Belov et al. 2001; Munini et al. 2018). The data collected by HEPD 02 will provide crucial insights into these phenomena, offering new perspectives on the dynamics of this phenomenon at MeV energies and underpinning

the development of more accurate theoretical/empirical models of the passage of the CME, thereby establishing the instrument as a possible key asset for advancing research in this field.

3.3 Energetic Particles Trapped in the Magnetosphere

The Van Allen belts (VABs) are two distinct regions of trapped charged particles encircling Earth, located within the inner magnetosphere. The inner belt, spanning roughly from 0.2 to 2 Earth radii (L values between 1.2 and 3), is densely packed with electrons reaching energies of hundreds of keV and protons exceeding 100 MeV, held in place by the comparatively stronger magnetic field of the region (Gusev et al. 2003). The outer belt, composed primarily of high-energy electrons (0.1–10 MeV), is more dynamic and responsive to solar activity, leading to greater variability than the inner belt (Shprits and Thorne 2004).

The dynamics of the charged particles inside the belts are controlled by the magnetic and electric fields in space and vary as a result of the interaction between the solar wind and the Earth's magnetic environment.

One of the most intriguing features associated with the Earth's radiation belts is the South Atlantic Anomaly (SAA), a region where the inner Van Allen radiation belt dips down to an altitude of about 200 kilometers. The anomaly is caused by the shift of the magnetic dipole axis with respect to the Earth axis, combined with anomalous current fluxes in the core-mantle boundary in the southern hemisphere.

Understanding the behavior of the VABs is crucial for space missions and satellite operations. During their orbits, the CSES satellites traverse the inner and outer VABs, as well as the SAA, collecting high-resolution particle measurements. These observations are sensitive to variations in the belts' shape and position over time (Bartocci et al. 2025b). Figure 6 displays simulations of belt electrons and protons (top and bottom panels, respectively), highlighting the distinct regions where these particles are concentrated. Simulations were carried out by means of the AE9/AP9 models of trapped particles via the IRENE software (version 1.58.001) (Ginet et al. 2013), averaging the integral omnidirectional fluxes of electrons above 3 MeV and protons above 30 MeV over a 3-months period between 2022-08-01 and 2022-10-31.

The physics of the Earth's inner radiation belt was investigated by HEPD-01 in Martucci et al. (2021, 2022), where an estimation of the trapped proton populations was given as a function of energy, pitch angle and L-shell in the 2018-2021 period, showing good agreement with the NASA AP9 model (Ginet et al. 2013).

The low-energy data collected by HEPD-01 allowed also to assess the drift of the SAA with notable accuracy, with unique coverage of time, altitude, and energy range (Bartocci et al. 2025b). More recently, HEPD-01 analyzed the trajectories of sub-250 MeV reentrant albedo protons in Low-Earth Orbit, evaluating the stability of these populations over time and confirming results from previous missions like PAMELA and AMS-01 (Martucci et al. 2024). It also captured notable changes in low-energy particle distributions within the Earth's magnetosphere during major geomagnetic storms in August 2018 (Palma et al. 2021b) and May 2021 (Piersanti et al. 2022).

Due to their stability and precision, the CSES particle detectors, HEPD-01 and HEPD-02, are well-suited to monitor the evolution of these particle populations — from gradual processes like solar modulation (Bruno et al. 2021) to rapid disturbances driven by geomagnetic storms, which can significantly reshape trapped particles at medium to high latitudes.

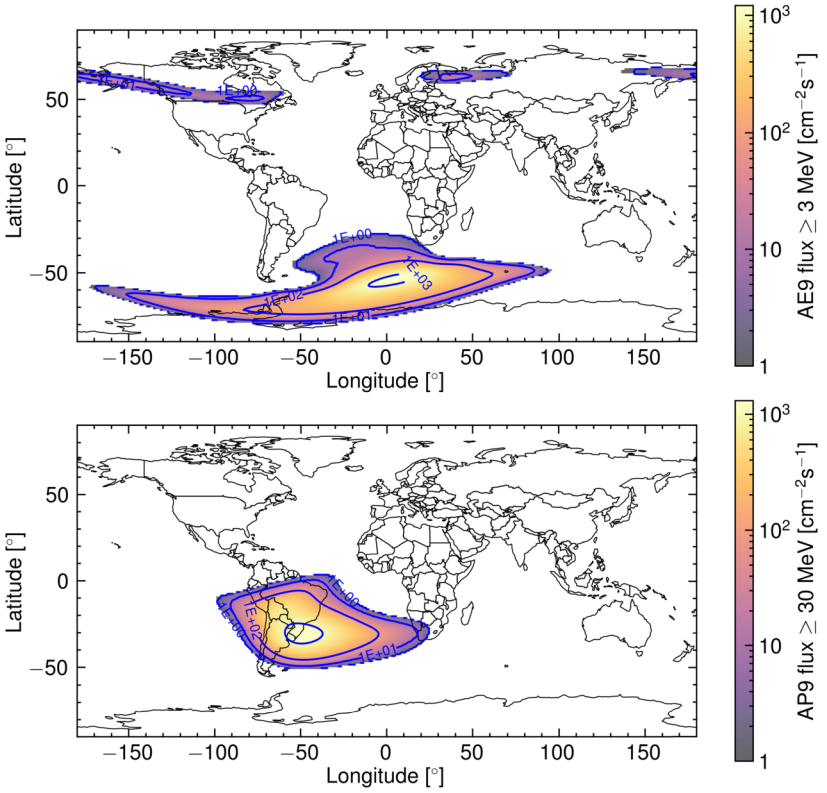

Fig. 6 Expected flux of electrons (top panel) and protons (bottom panel) from radiation belts, as detectable by the HEPD-02 instrument. Estimates were computed by relying on the AE9/AP9 models of trapped radiation (Ginet et al. 2013). The model integral omnidirectional fluxes above a given energy were averaged over 1400 realistic CSES-02 orbits, obtained by numerically propagating the trajectory from TLE data of CSES-01. The energy thresholds for electrons and protons are 3 MeV and 30 MeV, respectively, as reported in the colorbars

3.4 Particle Bursts

Precipitations of electrons and protons can be observed by satellite detectors as sudden increases in particle fluxes lasting from a few to tens of seconds. Particle bursts (PBs) are defined as anomalous rises in count rates exceeding typical background fluctuations. Several phenomena may cause these bursts, including whistlers, i.e. very low frequency (VLF) electromagnetic waves produced by lightning, artificial radio emissions, nuclear explosions capable of creating long-lived artificial radiation belts, and volcanic activity.

Over the past two decades, notable progress has been made in studying particle precipitations (e.g. Summers and Thorne 2003; Summers et al. 2007; Miyoshi et al. 2015, 2008; Nakamura et al. 2019), and interest in PBs correlated with seismic events (e.g. Aleksandrin et al. 2003; Bakaldin et al. 2007; Fidani et al. 2010; Battiston and Vitale 2013) or as potential seismic precursor signals (e.g. Sgrigna et al. 2005, and references therein) has grown. These bursts, often linked to major seismic events, provide valuable insights into the coupling mechanisms between the lithosphere, atmosphere, and ionosphere. Analysis

of SAMPEX satellite data by Sgrigna et al. 2005 suggests that PBs may act as short-term seismic precursors, appearing approximately four hours before large earthquakes.

This field of research holds promise for improving our ability to predict and respond to natural disasters, thereby enhancing public safety and preparedness.

HEPD-01 carried out extensive searches for PBs potentially linked to earthquakes. However, its sensitivity proved insufficient to draw definitive conclusions on such a complex topic. With data from both CSES missions, a significant boost in sensitivity is expected. The enhanced particle identification and pitch angle measurements of HEPD-02, combined with over a decade of total observation time, could finally allow the HEPD instruments to confirm or challenge previous findings on PB-like earthquake precursors.

3.5 Astrophysics of the Milky Way and Beyond

Gamma-ray bursts (GRBs) are among the most energetic events in the known Universe, unleashing powerful surges of photons that eventually reach the Earth following a long travel through space. Due to their neutral nature, they are unaffected by magnetic fields, and their minimal interaction with interstellar matter makes the Universe itself essentially transparent to them. Analyzing the attributes of these events (such as temporal patterns and energy spectra) has proven pivotal in unraveling the origins of GRBs and formulating models for the relativistic emission processes involved in these phenomena.

The HEPD-01 and the low-energy detector of the High-Energy Particle Package (HEPP-L) (Li et al. 2019) instruments onboard CSES-01 were capable to detect Gamma-Ray Bursts as an excess of low-energy electrons (by product of the photon interaction with the upper layers of the detector) a few seconds after the occurrence of these astrophysical events (Battiston et al. 2023; Palma et al. 2021a; Bartocci et al. 2024b).

The upgraded capabilities of HEPD-02 in GRB detection make it a valuable addition to current GRB observatories operating in the MeV energy range, such as Swift/BAT (Barthelmy et al. 2005)and Fermi/GBM (Meegan et al. 2009). While HEPD-02 does not target a new energy domain, its contribution lies in strengthening the global GRB monitoring network: due to Earth occultation and orbital constraints, any individual low-Earth-orbit satellite has limited instantaneous sky coverage, and the presence of additional MeV detectors significantly increases the probability of detecting prompt GRB emission and ensures more uniform temporal and directional coverage. Furthermore, HEPD-02's operation during a period overlapping the end of O4 and the start of O5 — the observing runs of the Laser Interferometer Gravitational-Wave Observatory (LIGO)/Virgo gravitational wave detectors — presents an exceptional opportunity for multimessenger astrophysics, enhancing the potential for joint observations of high-energy particles and gravitational waves.

3.6 Background for Indirect Dark Matter Searches

The possible presence of antideuterons and antihelium nuclei in the galactic environment is a strong signature in favour of dark matter (DM), due to the absence of such particles from purely astrophysical background (Korsmeier et al. 2018). Below 1 GeV, understanding solar modulation effects is crucial, since a detailed understanding of solar physics and in general low-energy backgrounds could be of uttermost importance in catching small,"exotic" effects (Giesen et al. 2015). HEPD-02 is sensitive exactly in this energetic regime and, therefore, a complete and highly precise proton spectrum determination is extremely valuable.

For instance, any observation of the balloon-borne General AntiParticle Spectrometer (Rogers et al. 2023) would greatly benefit from simultaneous HEPD-02 observations,

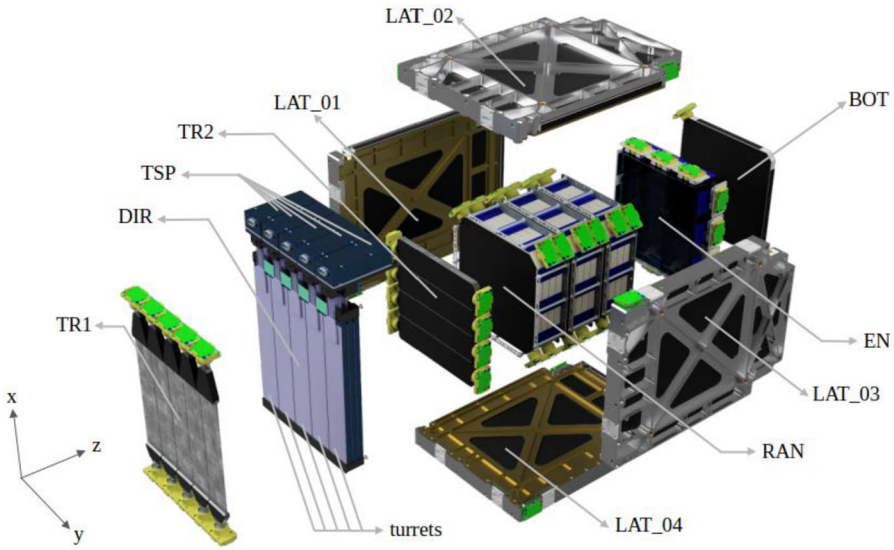

Fig. 7 Exploded CAD (computer-aided design) rendering of the HEPD-02 instrument. See the text for details

Table 2 List of HEPD-02 key target performances and operational specifications

Parameter	Value
Kinetic energy range (e^-)	3 MeV to 100 MeV
Kinetic energy range (p)	30 MeV to 200 MeV
Angular resolution	$\leq 10°$ (e^-, $E_{kin} = 10$ MeV)
Energy resolution	$\leq 25\%$ (e^-, $E_{kin} = 10$ MeV)
Operating temperature	-10 °C to $+35$ °C
Operating pressure	$\leq 6.65 \times 10^{-3}$ Pa ("vacuum")
Dimensions	53 cm × 39 cm × 37 cm
Mass	47 kg
Max. power consumption	43 W
Data budget	≤ 100 Gbit/day
Life span	> 6 years
Operation duty cycle	Full time operational

which could help discriminate a genuine exotic signal from confounding factors such as small SEP injections or other transient events that are common near the peak of the solar cycle.

4 HEPD-02 Structure and Operation

The structure of HEPD-02 instrument is shown in Fig. 7, while the target performances and operational specifications are summarized in Table 2. These parameters define the energy range, resolution, detection efficiency and operational constraints, ensuring the suitability for the intended measurements.

Table 3 List of the Italian facilities, particles and energies used for the calibration campaign of HEPD-02

Facility	Particle	Kinetic energy
LINAC of Santa Chiara Hospital, Trento (Mohamed et al. 2018)	electrons	6, 9, 12 MeV
LINAC of Santa Chiara Hospital, Trento (Mohamed et al. 2018)	gamma rays	up to 12 MeV
APSS Proton Therapy Center, Trento (Tommasino et al. 2017)	protons	from 30 to 228 MeV
Beam Test Facility, Frascati (Di Giulio et al. 2022)	electrons	from 30 to 450 MeV
CNAO, Pavia (Rossi 2011)	carbon nuclei	from 115 to 398 MeV/amu

During orbital flight, the instrument is oriented in zenithal direction with the z-axis points toward Earth; incoming particles from outer space enter the first trigger layer TR1 (described in 4.1) and cross the direction detector DIR (see 4.2), which reconstructs the incoming direction. The DIR is followed by a second trigger layer TR2 (also described in 4.1) and by the calorimeter (see 4.3), composed of a light section (RAN) and a heavy one (EN), where the particles lose most of their energy. The containment detector, made of bottom (BOT) and lateral (LAT) layers as described in Sect. 4.4, allows tagging of events not fully contained in the inner detectors. The direction detector employs monolithic active pixel sensor (MAPS) while the other detectors employ scintillators read-out by photomultiplier tubes (PMTs) (Bartocci et al. 2024c).

To estimate the expected performance of HEPD-02, a Monte Carlo (MC) simulation was developed based on the GEANT4 toolkit (Agostinelli et al. 2003). The geometry of the detector was imported in the simulation exporting the CAD mechanical model from the STEP (STandard for the Exchange of Product model data) format to GDML (Geometry Description Markup Language) format (Chytracek et al. 2006) using the GUIMESH tool (Pinto and Gonçalves 2019). The GDML format is then automatically parsed and loaded by the GEANT4 Detector Geometry classes, providing a detailed version of the detector geometry. Moreover, dedicated software developments were carried out to accurately simulate the digital output of the HEPD-02 scintillators (Bartocci et al. 2026b) and pixel sensors to the passage of particles (Bartocci et al. 2025c).

The actual performances were assessed by collecting experimental data during a beam test campaign at several facilities, listed in Table 3 along with the available particles species and energy ranges. The comparison with the experimental data allowed a fine tuning of the simulation parameters.

The overall thickness of the detectors along the z axis amounts to 5.0 radiation lengths and to 0.4 nuclear interaction lengths, which are dominated by the EN section (4.3 radiation lengths and 0.3 interaction lengths). The cumulative lengths crossed by particles as a function of the penetration depth are shown in Fig. 8. This figure clearly shows the concept at the basis of the instrument design: the combined TR1 and DIR overall material budget was set to the minimum allowed by other design constraints, thus enabling the lowest-energy particles of interest to enter also TR2 and the following layers for adequate triggering and measurement of released energy; the high-density EN section at the bottom is aimed at containing particles of higher energies.

The mechanical layout of the whole payload is presented in Fig. 9. The payload Al-alloy container box is composed of a base plate for mechanical and conductive thermal coupling with the satellite and, in addition, of 5 panels, 2.5 mm thick, externally treated with conductive black coating. The top panel contains the external connectors for power and signal cabling toward the satellite. The lateral panel adjacent to TR1 includes a rectangular hole where a thin particle entrance window made of copper-clad polyimide layer (18 μm

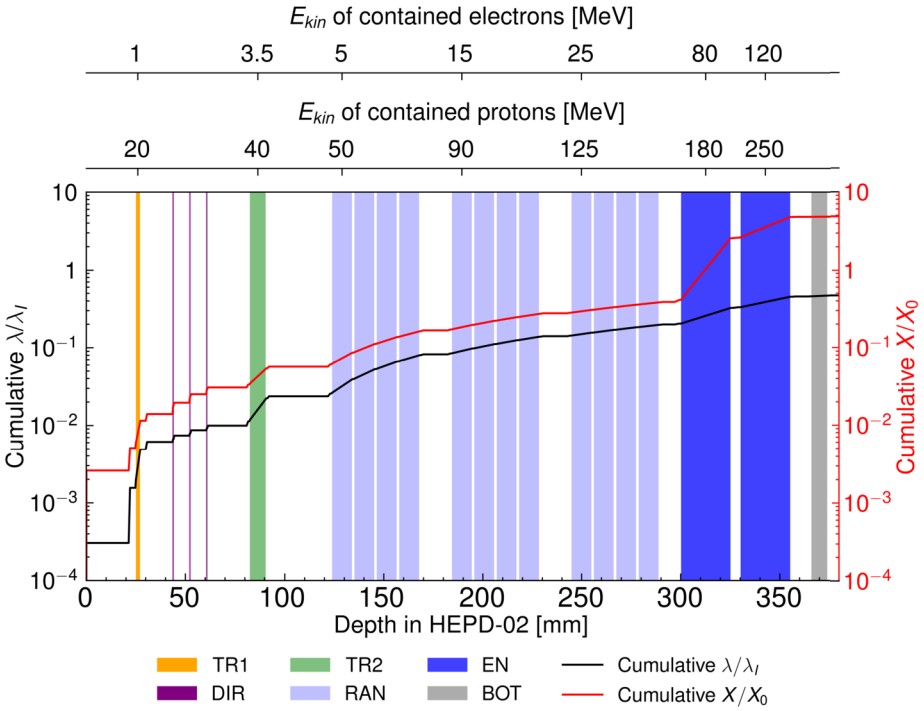

Fig. 8 Cumulative radiation length (X/X_0, red curve) and nuclear interaction length (λ/λ_I, black curve) as functions of depth along the HEPD-02 instrument z axis, obtained with MC simulation considering both active and inactive materials. Vertical color-coded regions represent active layers, with DIR thickness not drawn in scale for visualization purposes. Horizontal axes on top indicate the kinetic energy (E_{kin}) for which the 95% of electrons or protons are contained up to the corresponding depth

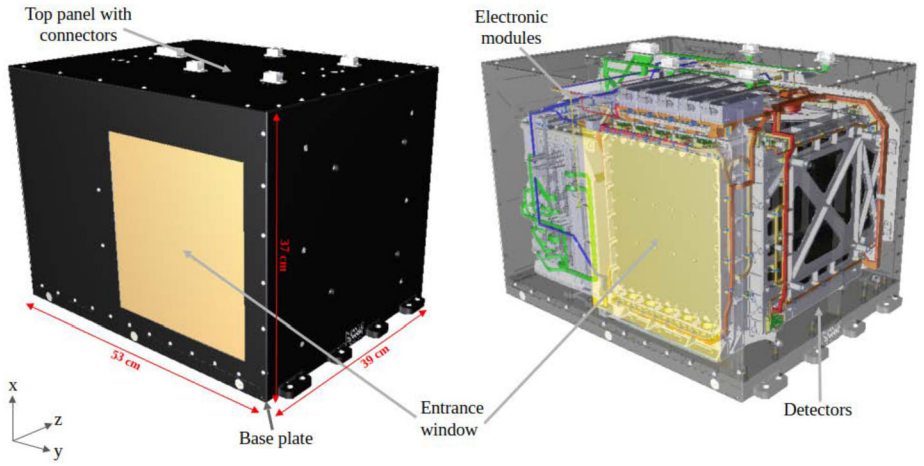

Fig. 9 CAD rendering of the HEPD-02 payload with the container box (left) and without it (right)

polyimide + 50 μm copper + 18 μm polyimide) is installed, in order to minimize the amount of material crossed by particles before reaching the instrument.

The read-out, control and power electronics are composed of specific units. They are packed as a stack of modules on the side of the instrument. Each board is implemented in two copies, following a cold redundancy architecture, with a main board normally operated and a spare one kept off: in case of malfunctioning, the role can be reversed. Upon transition to the spare side, all electronic boards are automatically switched over to the spare part to ensure system continuity.

The system configuration, control and data interfaces with satellite are managed by the Data Processing and Control Unit (DPCU). The DPCU exchanges data with the other HEPD-02 units via full-duplex SpaceWire Lite dedicated links; it is connected with the satellite by means of a CAN bus for slow control (incoming telecommands or broadcasts and outgoing telemetries) and a RS422 link for transmission of the scientific data collected by HEPD-02.

The system power is managed by a low-voltage power supply (LV-PS) unit through DC voltage conversion from the 29.5 V power line delivered by satellite (Bartocci et al. 2025a). The LV-PS manages the initial power-on sequence for correct DPCU board start-up and implements voltage monitor and current limit/monitor functionalities on power lines. The LV-PS also manages single-line telecommand inputs from satellite (on, off, stand-by) and telemetry outputs (power bus voltage monitor, temperatures monitor, error condition).

The following sections describe the main features of HEPD-02 detectors, the preliminary assessment of their relevant performances obtained by means of beam tests and simulations, the operational strategies; a final section briefly describes the HEPD-02 test campaigns before launch.

4.1 Trigger Detector

The trigger detector consists of TR1 and TR2, two rectangular layers of plastic scintillator Eljen EJ-200 (EJ200 2021), segmented in bars read-out by two PMTs at the opposite ends.

The employed PMTs, Hamamatsu R9880-210, are the same for all the scintillator modules of HEPD-02 (see also 4.3 and 4.4). They are characterized by 8 mm photocatode diameter and gain set in the range from 0.5×10^6 to 3×10^6 according to the light yield of each scintillator module. Their quantum efficiency is specifically high (30% to 40%) in the range of wavelengths between 400 and 450 nm, corresponding to the bulk of emission from the HEPD-02 scintillator, with peak wavelength ∼420 nm. The PMT bias voltages (up to ∼1000 V) are provided by the high-voltage power supply (HV-PS) unit (Bartocci et al. 2025a).

The first trigger plane TR1 is positioned before the direction detector. It is segmented into 5 bars of dimensions 32.5 mm × 154.5 mm. To match the side area of a bar with the PMT active area, UV-transparent polymethyl methacrylate (PMMA) light guides are placed at both ends. TR1 is 2 mm thick in order to minimize the energy loss of low-energy particles.

The second trigger plane TR2 is placed between the direction detector and the calorimeter. TR2 is segmented into 4 bars, oriented perpendicularly with respect to those of TR1. Each bar covers a surface of 36 mm × 150 mm. The thickness of TR2 (8 mm) was defined after optimizing the energy resolution obtained for minimum ionizing particles, and also taking into account the PMT photocatode diameter.

The overall design constitutes an improvement with respect to HEPD-01, which employed a single trigger plane: in fact, by requiring a trigger signal from both TR1 and TR2 (standard HEPD-02 trigger pattern), it is possible to acquire mostly events where the incoming particle trajectory enters the RAN detector. Each single TR1 and TR2 bar can be

inhibited from contributing to the trigger signal, thus drastically decreasing the effective acceptance and therefore the trigger rate if needed, for example in the case of a reduction of allocated daily data budget.

The analog signals produced by the 64 PMTs of all the scintillation detectors of HEPD-02 (see also 4.3 and 4.4) are managed by the trigger board (Anastasio et al. 2025), relying on Weeroc Citiroc 1A ASICs, ADCs and FPGA to generate digital samplings of the pulse amplitudes and trigger signals needed for starting and synchronizing HEPD-02 data acquisition. The trigger logics can be built up with different combinations of the 64 PMTs and with selectable pre-scaling; including the standard HEPD-02 trigger pattern mentioned above, a total of 10 trigger patterns are available: 9 pre-defined ones plus an additional one, reconfigurable also in flight. The board measures live and dead time between subsequent event triggers. The board also contains rate meters for single PMT signals and for the 10 trigger patterns, implementing continuous monitoring along the orbit. Drawing from the HEPD-01 experience, the counter for the trigger pattern with the lowest energy threshold (and consequently the highest rate) has been expanded from 16 to 20 bits to prevent overflows during passages through the SAA.

4.2 Direction Detector

The direction detector (DIR, or briefly "tracker") (Barioglio et al. 2025; Coli et al. 2022) is based on the monolithic active pixel sensor (MAPS) technology developed for ALICE (A Large Ion Collider Experiment) (Aglieri Rinella 2017). It constitutes a notable innovation with respect to HEPD-01, which employed two layers of double-sided Si microstrip sensors, and it marks a significant milestone as the first-ever employment of a silicon pixel tracker in space-based applications. It includes a total of 150 Tower Semiconductor ALTAI (Barioglio et al. 2025) MAPS (15 mm $\times$ 30 mm area), characterized by a 180 nm complementary metal-oxide-semiconductor (CMOS) process. The pixel size of 29.24 μm $\times$ 26.88 μm allows for a single hit resolution of approximately 4 μm with a noise rate as low as 10^{-10} fake hits/pixel/event.

The monolithic sensor includes the whole signal processing chain (hit detection, zero suppression and digital output) directly inside the active layer, leading to a more compact structure.

The DIR detector (see Fig. 10) is composed of 15 *staves*, each consisting of 10 ALTAI sensors arranged in two columns. The overall assembly is obtained by aligning five *turrets* side by side, with each turret formed by vertically stacking three staves and connecting them to the control and read-out electronics through a lateral tracker splitter (TSP) board. Each tracker plane is characterized by a 150 mm × 150 mm total active area. The three planes of MAPS allow for a minimum measurement redundancy and a direct monitoring of alignment and efficiency of single staves.

The tracker data acquisition (TDAQ) board (Bartocci et al. 2026a) manages the DIR detector configuration as well as the read-out and processing of pixel hit data, with a dedicated digital link for each of the 15 staves.

Figure 11 shows the preliminary performance in arrival direction identification, obtained with electron and proton beams of various energies. The arrival direction is reconstructed by using the information of close-by pixels activated by the particle passage, which are grouped in *clusters*. A fitting procedure uses the centers of gravity of these clusters to determine the arrival direction defined by the polar angle θ and the azimuthal one ϕ. Events are selected by requiring that at least one bar of TR1 and one bar of TR2 recorded a signal over threshold; to remove pile-up effects, only events with a single reconstructed track with a single cluster on each tracker layer are retained.

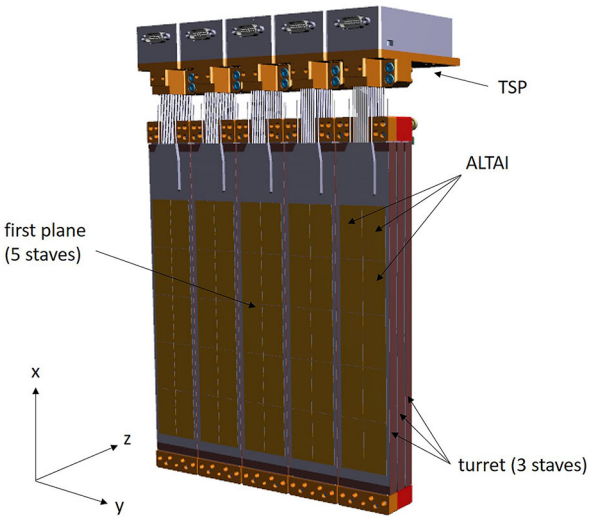

Fig. 10 CAD rendering of the DIR detector assembly, with the first of three planes in full view. Each plane is segmented into 5 adjacent staves, each one carrying 10 ALTAI sensors arranged in two columns

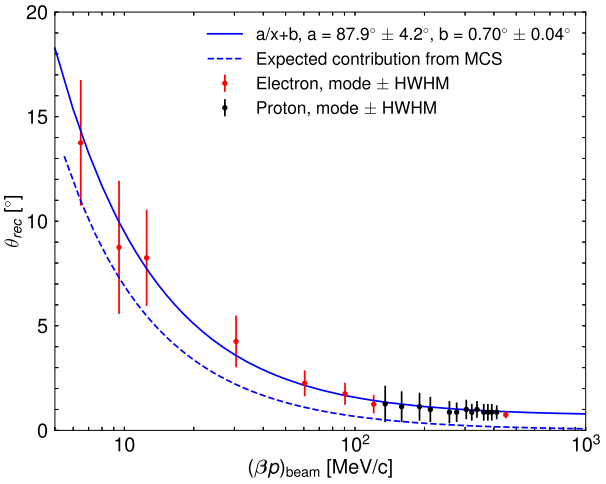

Fig. 11 Reconstructed polar angle θ_{rec} for beam particles as a function of $x = (\beta p)_{beam}$. The points represent the mode of the reconstructed polar angle distributions, while the error bars refer to their half-widths at half-maxima (HWHM). The solid blue line shows a fit of the dependence, while the dashed blue line shows the contribution expected from the MCS estimated with a Geant4 simulation of particles with a flat energy spectrum directed along the z axis of HEPD-02 (Bartocci et al. 2026b)

The energy dependence of the mode of the reconstructed polar angle θ_{rec} distribution is well described by the parameterized fit $a/x + b$ where $x = (\beta p)_{beam}$ expressed in MeV/c. Below 60 MeV/c, the multiple Coulomb scattering (MCS) dominates the tracking uncertainty over the intrinsic alignment of sensors. At higher energies, the asymptotic value b is dominated by the remaining relative misalignment between the HEPD-02 z-axis and the beam direction; consequently, it does not reflect the detector's internal alignment.

4.3 Calorimeter

The calorimeter consists of two sections. The first one is a tower of twelve EJ-200 plastic scintillator layers, effective to assess the penetration range of particles less energetic than 150 MeV/n and therefore collectively indicated as RAN (range sub-detector). The second one is composed of two layers of much heavier lutetium-yttrium oxyorthosilicate crystal (LYSO) scintillator bars, collectively indicated as EN (energy sub-detector).

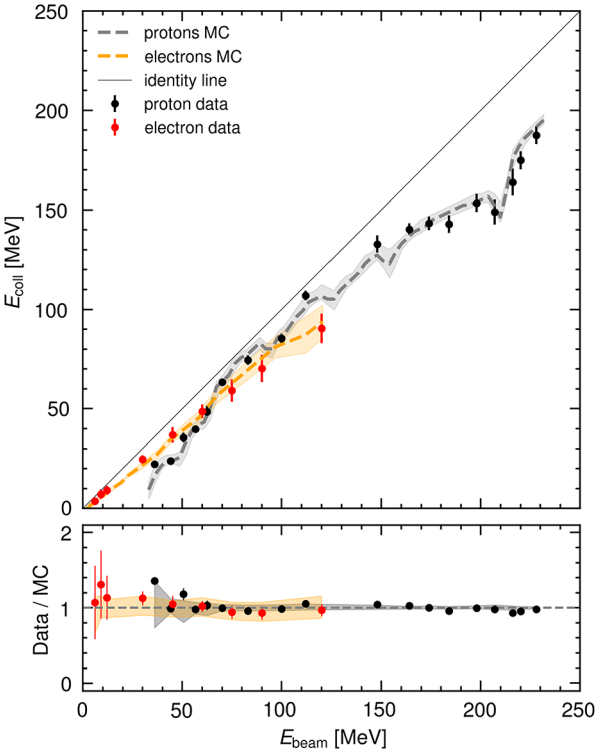

Fig. 12 Correlation plot between collected energy E_{coll} in TR1, TR2, RAN and EN layers and nominal beam energy E_{beam}, for electrons and protons. The shaded bands represent the MC prediction and are obtained, for each E_{beam}, from the lower and upper HWHM of the E_{coll} distribution around its mode. The identity line is also represented, with the purpose of showing the amount of missing energy, mostly due to deposit in inactive layers, which can be estimated and corrected for by means of the MC simulation

Each RAN layer has size 150 mm × 150 mm × 10 mm; it is read-out by two PMTs at opposite corners. For subsequent RAN layers, the PMTs are positioned alternatively on different diagonals, thus sampling the energy release with an overall uniform sensitivity in the xy plane, and at the same time allowing to maximize the compactness of the assembly along the z axis.

The 12 RAN layers are mechanically arranged in groups of 4, each group housed in an Al-alloy frame with top and bottom covers made of carbon fiber reinforced polymer (CFRP); this solution is an evolution with respect to the HEPD-01 design, where all planes were stacked in a unique frame: it increases the positional stability of each plane, while the CFRP covers introduce a tolerable additional amount of inactive material.

Each EN layer is made of three LYSO bars, characterized by quite a remarkable size for a space experiment (150 mm × 49 mm × 25 mm). Each bar is read-out by two PMTs placed at opposite ends; the bars of the two layers are mutually orthogonal.

The EN configuration has several advantages over the one adopted for HEPD-01, namely a single layer of 9 cubes with a single PMT positioned on the bottom side of each cube: the double PMT read-out of each bar, the removal of the PMT from the region crossed by particle trajectories, the segmentation in two layers that provides additional information along the z axis. This design reduces the inactive material between adjacent bars, compared to the LYSO cube matrix used in HEPD-01.

The preliminary energy measurement performance is shown in Fig. 12, as obtained with electron and proton beams incident on the TR1 layer, at the center and in one corner, respectively. The energy E_{coll} is obtained by summing the signal collected by each detector layer, which in this preliminary analysis is obtained by knowing the most probable value (MPV)

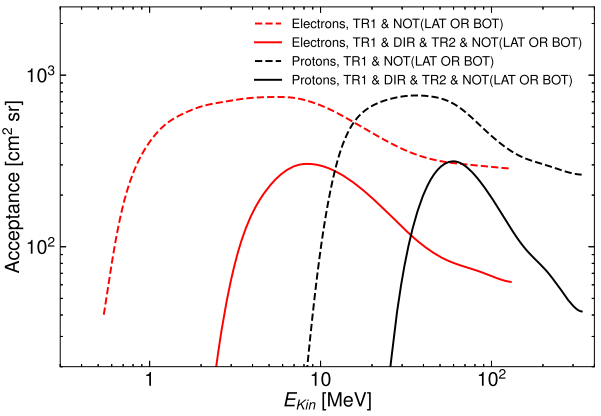

Fig. 13 Acceptance of HEPD-02 for electrons (red) and protons (black) as a function of initial kinetic energy, considering three different conditions for each particle species (see text for details)

of the deposited energy distribution for a vertical minimum ionizing particle, corresponding to 1.6 MeV/cm for EJ-200 scintillator and 9.3 MeV/cm for LYSO. The plot shows that most of particles' energy is deposited in scintillators, with negligible losses due to the mechanical structure of the apparatus. An accurate Monte Carlo simulation successfully reproduces such an effect, more important for protons and light nuclei than for electrons. Finally, exploiting the information from the direction detector, the kinetic energy of the impinging particle will be reconstructed with high-resolution all over the energy intervals reported in Table 2.

4.4 Containment Detector

The containment detector consists of five EJ-200 plastic scintillator layers surrounding the inner detectors (TR2, RAN and EN) on the bottom side (BOT) and on the lateral sides (LAT); each one is 8 mm thick and read-out by two PMTs located at opposite corners. Compared with HEPD-01, the mechanical design of BOT and LAT was completely revised to minimize the amount of inactive areas necessarily introduced by the mechanical holders for scintillators and PMTs.

The containment detector concurs to define the acceptance of the HEPD-02 apparatus, by tagging low-quality categories of events, such as particles crossing the trigger planes and not fully contained inside the calorimeter, which would lead to an underestimation of their energy. Another important category of tagged low-quality events are particles entering RAN or EN from lateral or bottom sides and not reaching the direction detector. Thanks to containment detector events with particles not fully contained will be discarded at analysis level.

A Geant4 simulation of electrons and protons with flat energy spectrum and isotropic angular distribution interacting with HEPD-02 was run to calculate the apparatus acceptance for the two particle species as a function of their kinetic energy, as shown in Fig. 13. The acceptance definition depends on the specific trigger condition among those that can be implemented during operation. Here two typical definitions are considered:

- particle crossing TR1 to give trigger therein: this condition is optimized to catch low-energy particles that stop in the first layers and do not reach TR2;
- particle crossing TR1, DIR and TR2, thus satisfying the standard HEPD-02 trigger pattern (signal from both TR1 and TR2) and being tracked.

The corresponding acceptances are defined by also requiring that no signal is recorded by LAT and BOT (containment condition).

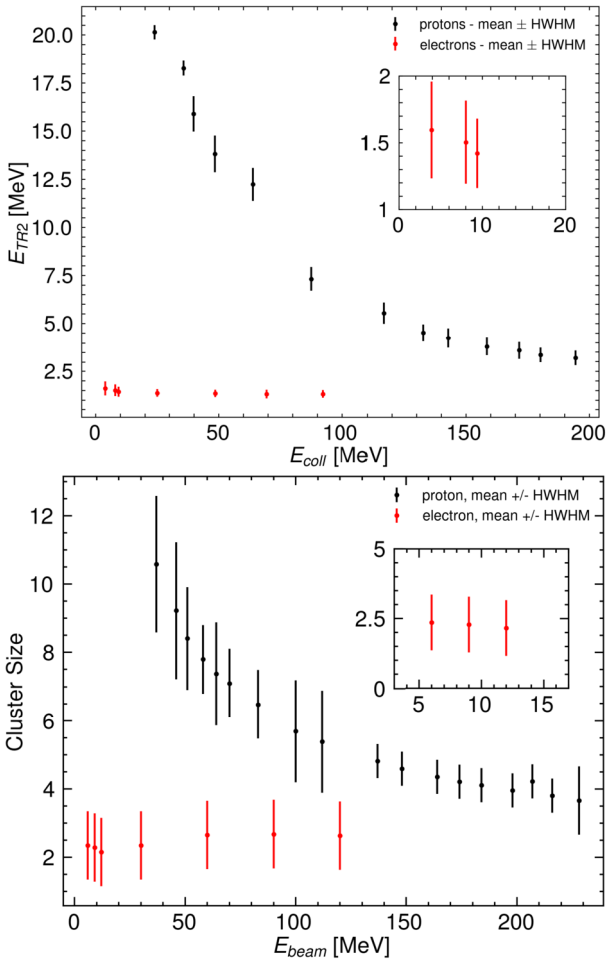

Fig. 14 Top: energy collected in TR2 vs. sum of energy collected in TR1, TR2, RAN and EN sensitive layers, for beams of protons and electrons of different kinetic energies, ranging from 6 to 120 MeV for electrons, and from 35 to 228 MeV for protons. Bottom: measured cluster size on any of the three tracker layers vs. beam energy for electrons and protons. The electron points below 15 MeV are also displayed in an inset to enhance clarity

The simulation confirms that the sensitivity range exceeds the design requirements for both particle types. The instrument achieves a peak acceptance of approximately 800 cm^2sr. The sharp increase of the detector acceptance at around 0.5 MeV and 10 MeV, respectively for electrons and protons, is due to the threshold effect for particles being absorbed in the entrance window, before reaching the TR1 bars. At 100 MeV and 200 MeV, respectively for electrons and protons, the acceptance starts decreasing, due to particles escaping from the inner detector layers and violating the containment condition. More details about the Geant4 HEPD-02 simulation can be found in (Bartocci et al. 2026b).

4.5 Particle Identification with HEPD-02 Detectors

Particle identification is a task that HEPD-02 can accomplish thanks to independent information coming from different detector units.

The top Fig. 14 illustrates a method of discrimination between protons and electrons that exploits the different dependence of the signal collected in the TR2 layer on the total energy released in TR1, TR2, RAN and EN. The bottom Fig. 14 shows an additional and independent discrimination method employing the size of pixel clusters formed on a tracker layer

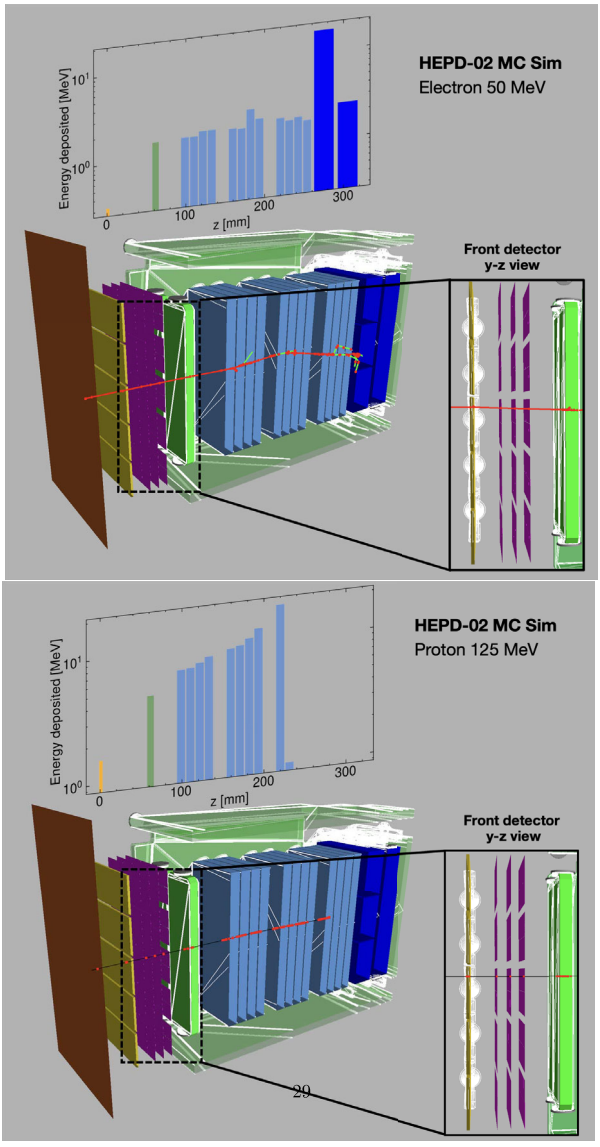

Fig. 15 Simulated event displays showing the detection of a 50 MeV electron (top) and a 125 MeV proton (bottom) inside the HEPD-02 apparatus, by means of cutaway planes. The red and black tracks respectively represent the trajectories of the electrons (primaries and secondaries) and protons, while the green tracks correspond to secondary photons produced in the interactions. Red circles indicate points where hits are registered within the detector. The brown layer depicts the HEPD-02 entrance window, followed by the active layers drawn with the same color scheme used in Fig. 8. The white wire-frames show some of mechanical structures within the detector. The energy deposit profile is shown in the histogram on top of the figure

vs. the kinetic energy of the particle. In both figures, the different behaviour of electrons and protons is due to the fact that, in the considered energy range, electrons are at minimum ionization while the much heavier protons are relatively slow and their energy release increases for lower energies according to the well known Bethe-Bloch formula.

Another crucial aspect for electron/proton discrimination is the significantly different energy deposition profile along the particle trajectory. The proton energy loss rate increases sharply as the particle slows down, leading to a Bragg peak (Bragg 1904) near the end of the particle range; on the other hand, contained electrons do not exhibit this feature and show a much more uniform energy deposition along their path. As an example, Fig. 15 illustrates the simulated detection of a 50 MeV electron (top) and a 125 MeV proton (bottom), both

being stopped in the calorimeter, with clearly visible Bragg peak for the proton. On the other hand, the electron energy release remains uniform while traversing the 12 plastic scintillator RAN planes, with an energy release per plane of approximately 2 MeV, a value close to that of a minimum ionizing particle; the peak observed in the first EN layer is caused by the interactions of secondary photons produced in the much denser LYSO material, leading to an enhanced energy deposition. These observables are exploited for particle separation during the ground analysis, after the raw binary data is down-linked and reconstructed. At this stage the data are calibrated (using ground and periodic in-flight calibrations) and then processed to reconstruct energy deposits and tracks and particle identity.

All these independent sources of information can be effectively combined using advanced techniques such as Multivariate Analysis (MVA) or Deep Learning (DL). These methods leverage the expertise gained from the HEPD-01 mission, where they were employed to enhance the particle identification capabilities and improve the overall performance of the detector (Bartocci et al. 2022).

4.6 In-Orbit Operational Strategies

The general in-orbit strategy of HEPD-02 follows the basic idea of its predecessor, HEPD-01. For most of the time, the detector operates in continuous acquisition mode along the orbit, with data being recorded in successive runs of approximately two minutes each. Short interruptions, typically occurring once per orbit in equatorial regions with low trigger rates, are required for in-flight calibrations, including the mapping of noisy pixels in the direction detector and the calculation of pedestals for the PMT read-out channels.

During acquisition mode, particle events that meet the active trigger conditions are processed and an event packet are generated by combining the detectors information with additional auxiliary data, such as live time/dead time, event timing, etc. In addition to this single-event acquisition, the rate meters in the trigger board allow to count incoming particles satisfying the 10 possible trigger patterns, independently of whether each pattern is active or not. As an example, Fig. 16 shows the expected rate for the HEPD-02 standard trigger pattern, as a function of time, along a descending-latitude orbit, according to the known particle population of radiation belts; a possible superposed particle burst of different origin is also represented, to show the way it can be clearly identified by the rate meter.

CSES-02 operates along the whole orbit, up to latitudes of 82.6°, while CSES-01 is kept in stand-by mode above 65°. This added possibility of continuous data collection in the polar regions allows a more comprehensive investigation of the outer radiation belt - which at the CSES-02 altitude extends in the latitude range from 45° to 85° in both the northern and southern hemispheres - by measuring particle composition and variations in response to solar events such as geomagnetic storms.

The expanded scientific capabilities required modifications to the in-orbit operational strategy with respect to HEPD-01, leading to the introduction of automatic adjustment of instrument configuration based on the satellite's position along the orbit, according to a latitude-longitude map that is partitioned into 16×8 cells (each corresponding to about 3 minutes of flight) to take into account the different particle populations encountered. It is also possible to simultaneously activate different trigger patterns tailored for specific objectives, such as different types of incoming particles or monitoring of various instrument performances.

During flight, the DPCU automatically sets the HEPD-02 configuration according to the orbital coordinates at hand. All the configuration parameters for each orbital cell are loaded into the DPCU memory and, most importantly, they can be adjusted via telecommands from

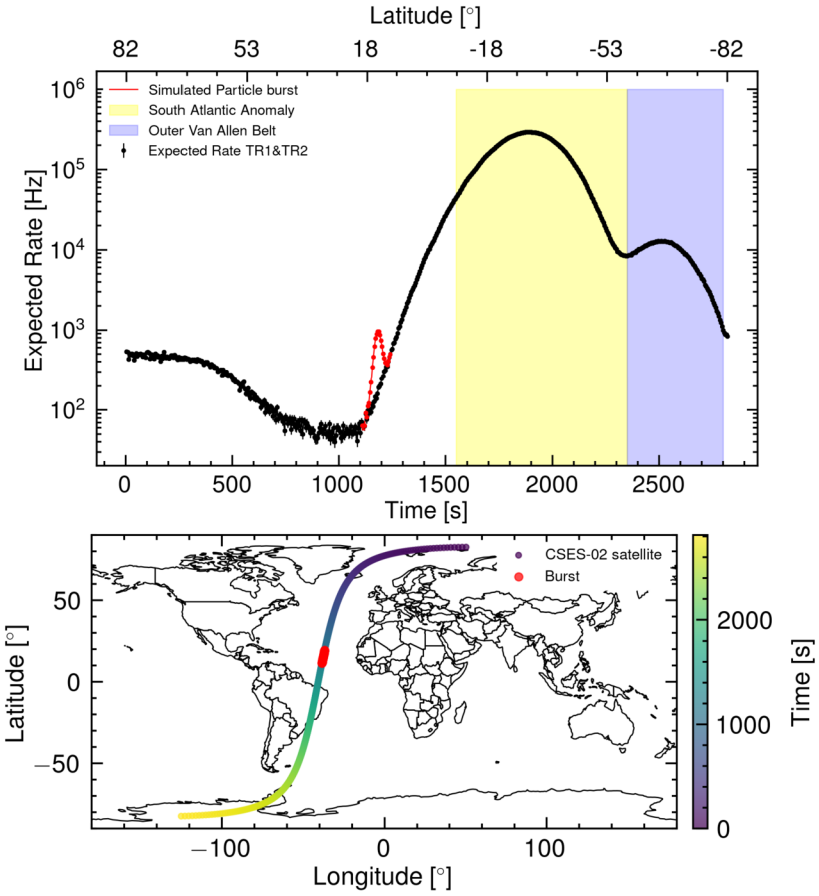

Fig. 16 Expected rate vs. time for the HEPD-02 standard trigger pattern (signal from both TR1 and TR2, top figure), along the specific descending-latitude orbit (bottom). The black points take into account the particle population of radiation belts; the red points in both figures represent the possible occurrence of a particle burst

ground. This flexibility allows to start operation with a conservative configuration (also to prevent saturation of data budget) and then tune the parameters depending on the analysis of the first flight data or evolving scientific objectives.

The simultaneous activation of multiple trigger patterns could result in data generation exceeding the daily data budget allocated to HEPD-02 within the satellite storage. This is particularly significant for those cells characterized by high particle fluxes, such as in the SAA or in the polar regions. Additionally, for some of these cells, a high acquisition rate for a particular type of trigger can overcome much less frequent concurrent trigger patterns. For all of these reasons, configurable pre-scaling is implemented in the trigger board logics. For each geographic cell, up to 6 concurrent trigger patterns can be activated, with 4 of them pre-scalable, with different factors for passages characterized by ascending or descending latitude.

As mentioned in Sect. 3.5, HEPD-01 was also able to detect several powerful GRBs. Building on this, HEPD-02 introduces a completely new detection mode specifically de-

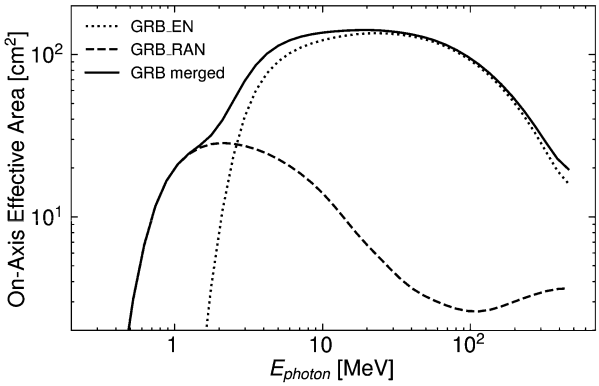

Fig. 17 HEPD-02 effective area for on-axis photons as a function of energy, for the single trigger patterns GRB_RAN and GRB_EN and for their combination. A peak value at 143 cm^2 is reached at a photon energy of approximately 20 MeV

signed for GRB observation. This feature operates independently from the standard event acquisition and relies on the continuous evaluation by the DPCU of the running average of the rate meters for two trigger patterns specifically designed for GRB detection, GRB_RAN and GRB_EN. These two patterns respectively involve signals from central RAN unit (or EN detector) with no hits on the respectively surrounding scintillators, for charged particles rejection. A dedicated algorithm generates a GRB-specific trigger in the case of increase in either of these two rates with high enough amplitude and rapidity.

The resulting dedicated GRB data acquisition mode is characterized by a fine 200 Hz sampling of the above mentioned rate meters; this mode is stopped when the rate surge disappears or within a few minutes, to comply with the maximum data budget.

The automatic setting of the HEPD-02 configuration also inhibits the GRB algorithm for latitude-longitude cells where a significant occurrence of sharp transients in charged particle rates is expected, resulting in false GRB triggers.

The effective on-axis area for the two patterns is shown in Fig. 17.

4.7 HEPD-02 Qualification and Acceptance Campaigns

In compliance with the mission requirements, two identical HEPD-02 models were assembled in the clean rooms in INFN at Roma Tor Vergata (Italy): a Qualification Model (QM) and a Flight Model (FM, see Fig. 18 and 19) that was thereupon integrated on satellite.

Both QM and FM underwent successful qualification and acceptance campaigns, followed by instrument calibration with beam tests and acquisition of cosmic rays at ground level.

The acceptance campaign of HEPD-02 FM was performed from February to July 2023 at the SERMS Laboratory in Terni (Italy) with vibration tests followed by thermal cycling in air and vacuum. This campaign was followed by extensive electromagnetic compatibility (EMC) measurements carried out in the anechoic chamber at the Institute of Applied Physics "Nello Carrara" (IFAC) of the National Research Council (CNR).

The FM was exposed, along the three axes, to vibrations with sinusoidal stimulus (10 - 100 Hz, intensity up to 8 G) and random loading (10 - 2000 Hz, with overall RMS value of 7.6 G). The FM was then extensively tested in a climatic chamber at standard pressure: 14.5 temperature cycles were performed between -20 °C and $+45$ °C, hence in a broader temperature range than specified in the operational requirements (-10 °C and $+35$ °C). Thereupon, 3.5 temperature cycles were performed in a thermal-vacuum chamber with the same temperature range, at a pressure $< 6.65 \cdot 10^{-3}$ Pa.

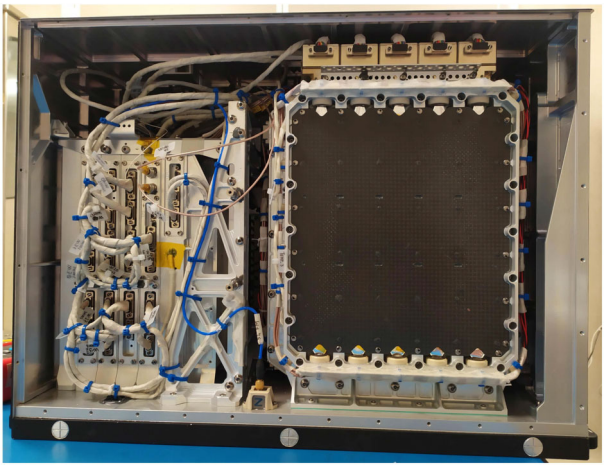

Fig. 18 The assembled HEPD-02 Flight Model, with the front panel removed

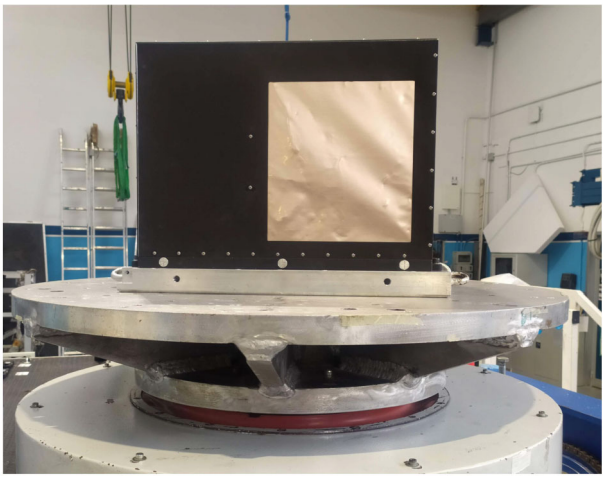

Fig. 19 The assembled HEPD-02 Flight Model during vibration test

No structural damages, EMC incompatibility, loss of functionality or scientific performance degradation were observed during or after the instrument qualification and acceptance campaigns. Therefore, in December 2023 the HEPD-02 FM was shipped to DFH Satellite Co., Ltd. in Beijing (China) for satellite integration.

In January 2024, upon completing stand-alone integrity verifications and magnetic cleanliness measurements, the HEPD-02 was installed on board CSES-02 and the compatibility of the electrical and data interfaces with the satellite was verified; in February 2024 a full functional test campaign was performed, followed in March 2024 by EMC and orbital maneuver tests conducted at the satellite level.

Between April and February 2025, the assembled CSES-02 satellite underwent a vibration test campaign, including both sinusoidal and random stimuli, a thermal balance test (two days) followed by 4 thermal-vacuum cycles (four days), a magnetic cleanliness test, an aging test with continuous operation for 5 days, a final functional verification including the telecommand sequences intended to be used during health check phase immediately after first power-on in orbit.

No anomalies were detected during the test campaign at DFH. Therefore, in May 2025, CSES-02 was transferred to the Jiuquan Satellite Launch Center (JSLC) in Gansu, Inner Mongolia, China. At JSLC, the procedures to be executed after the first power-on in orbit were tested as part of the final verification before the installation of CSES-02 on the Long March 2D rocket.

5 Conclusions

The scientific program of CSES involves the creation of a constellation of satellites. It will measure fields and plasma currents, as well as energetic charged particles in the Earth's magnetosphere, to study perturbations in the near-Earth radiation environment. The first mission, CSES-01, launched in 2018, is still collecting data. The second mission, CSES-02, was launched into orbit on June 14, 2025.

The Italian Limadou collaboration has built the High-Energy Particle Detector (HEPD) onboard the CSES satellites. This article describes the scientific potential and observational capabilities of HEPD-02, the version of the detector that is on board CSES-02.

HEPD-02 measures fluxes of particles, such as electrons, protons and nuclei. The science potential of the detector is wide, covering cosmic-rays science as well as solar and magnetospheric physics. In addition, it has sensitivity to gamma-ray bursts.

The increased coverage, the excellent spatial resolution for tracking and the good geometric acceptance of HEPD-02 will improve the data gathering power of the mission. A detailed Monte Carlo simulation was developed and an extensive beam test campaign was performed to validate HEPD-02 capabilities in identifying and measuring the kinetic energy and arrival direction of incoming particles. The performance of the instrument confirms that HEPD-02 is able to achieve the scientific objectives of the project.

All calibrated data from the CSES-02 payloads, including HEPD-02, will be made publicly available once the commissioning phase has been successfully completed and the cross-validation with data from other onboard instruments, as well as from independent satellite and ground-based sources, has been finalized. The datasets will be released through dedicated Italian and Chinese data portals.

Acknowledgements This work was supported by the Italian Space Agency (ASI) in the framework of the "Accordo attuativo 2019-22-HH.0 Programma Limadou-2 attività di fase B2/C/D/E1" and the ASI-INFN agreement n. 2021-43-HH.0.

Funding Information Open access funding provided by Università degli Studi di Trento within the CRUI-CARE Agreement. Open access funding provided by INFN and ASI.

Data Availability Not applicable.

Materials Availability Not applicable.

Code Availability Not applicable.

Declarations

Ethics Approval and Consent to Participate Not applicable.

Consent for Publication Not applicable.

Competing Interests The authors have no competing interests to declare that are relevant to the content of this article.

References

Aglieri Rinella G (2017) The ALPIDE pixel sensor chip for the upgrade of the ALICE Inner Tracking System. Nucl Instrum Methods Phys Res, Sect A, Accel Spectrom Detect Assoc Equip 845:583–587. https://doi.org/10.1016/j.nima.2016.05.016. Proceedings of the Vienna Conference on Instrumentation 2016

Agostinelli S, Allison J, Amako K, Apostolakis J, Araujo H, Arce P, Asai M, Axen D, Banerjee S, Barrand G, Behner F, Bellagamba L, Boudreau J, Broglia L, Brunengo A, Burkhardt H, Chauvie S, Chuma J, Chytracek R, Cooperman G, Cosmo G, Degtyarenko P, Dell'Acqua A, Depaola G, Dietrich D, Enami R, Feliciello A, Ferguson C, Fesefeldt H, Folger G, Foppiano F, Forti A, Garelli S, Giani S, Giannitrapani R, Gibin D, Gómez Cadenas JJ, González I, Gracia Abril G, Greeniaus G, Greiner W, Grichine V, Grossheim A, Guatelli S, Gumplinger P, Hamatsu R, Hashimoto K, Hasui H, Heikkinen A, Howard A, Ivanchenko V, Johnson A, Jones FW, Kallenbach J, Kanaya N, Kawabata M, Kawabata Y, Kawaguti M, Kelner S, Kent P, Kimura A, Kodama T, Kokoulin R, Kossov M, Kurashige H, Lamanna E, Lampén T, Lara V, Lefebure V, Lei F, Liendl M, Lockman W, Longo F, Magni S, Maire M, Medernach E, Minamimoto K, Mora de Freitas P, Morita Y, Murakami K, Nagamatu M, Nartallo R, Nieminen P, Nishimura T, Ohtsubo K, Okamura M, O'Neale S, Oohata Y, Paech K, Perl J, Pfeiffer A, Pia MG, Ranjard F, Rybin A, Sadilov S, Di Salvo E, Santin G, Sasaki T, Savvas N, Sawada Y, Scherer S, Sei S, Sirotenko V, Smith D, Starkov N, Stoecker H, Sulkimo J, Takahata M, Tanaka S, Tcherniaev E, Safai Tehrani E, Tropeano M, Truscott P, Uno H, Urban L, Urban P, Verderi M, Walkden A, Wander W, Weber H, Wellisch JP, Wenaus T, Williams DC, Wright D, Yamada T, Yoshida H, Zschiesche D (2003) Geant4—a simulation toolkit. Nucl Instrum Methods Phys Res, Sect A, Accel Spectrom Detect Assoc Equip 506(3):250–303. https://doi.org/10.1016/S0168-9002(03)01368-8

Aguilar M, Ali Cavasonza L, Ambrosi G, Arruda L, Attig N, Aupetit S, Azzarello P, Bachlechner A, Barao F, Barrau A, Barrin L, Bartoloni A, Basara L, Başeğmez-du Pree S, Battarbee M, Battiston R, Becker U, Behlmann M, Beischer B, Berdugo J, Bertucci B, Bindel KF, Bindi V, Boella G, de Boer W, Bollweg K, Bonnivard V, Borgia B, Boschini MJ, Bourquin M, Bueno EF, Burger J, Cadoux F, Cai XD, Capell M, Caroff S, Casaus J, Castellini G, Cervelli F, Chae MJ, Chang YH, Chen AI, Chen GM, Chen HS, Cheng L, Chou HY, Choumilov E, Choutko V, Chung CH, Clark C, Clavero R, Coignet G, Consolandi C, Contin A, Corti C, Creus W, Crispoltoni M, Cui Z, Dai YM, Delgado C, Della Torre S, Demakov O, Demirköz MB, Derome L, Di Falco S, Dimiccoli F Díaz C, von Doetinchem P, Dong F, Donnini F, Duranti M, D'Urso D, Egorov A, Eline A, Eronen T, Feng J, Fiandrini E, Finch E, Fisher P, Formato V, Galaktionov Y, Gallucci G, García B, García-López RJ, Gargiulo C, Gast H, Gebauer I, Gervasi M, Ghelfi A, Giovacchini F, Goglov P, Gómez-Coral DM, Gong J, Goy C, Grabski V, Grandi D, Graziani M, Guo KH, Haino S, Han KC, He ZH, Heil M, Hoffman J, Hsieh TH, Huang H, Huang ZC, Huh C, Incagli M, Ionica M, Jang WY, Jinchi H, Kang SC, Kanishev K, Kim GN, Kim KS, Kirn T, Konak C, Kounina O, Kounine A, Koutsenko V, Krafczyk MS, La Vacca G, Laudi E, Laurenti G, Lazzizzera I, Lebedev A, Lee HT, Lee SC, Leluc C, Li HS, Li JQ, Li JQ, Li Q, Li TX, Li W, Li Y, Li ZH, Li ZY, Lim S, Lin CH, Lipari P, Lippert T, Liu D, Liu H, Lordello VD, Lu SQ, Lu YS, Luebelsmeyer K, Luo F, Luo JZ, Lv SS, Machate F, Majka R, Mañá C, Marín J, Martin T, Martínez G, Masi N, Maurin D, Menchaca-Rocha A, Meng Q, Mikuni VM, Mo DC, Morescalchi L, Mott P, Nelson T, Ni JQ, Nikonov N, Nozzoli F, Oliva A, Orcinha M, Palmonari F, Palomares C, Paniccia M, Pauluzzi M, Pensotti S, Pereira R, Picot-Clemente N, Pilo F, Pizzolotto C, Plyaskin V, Pohl M, Poireau V, Putze A, Quadrani L, Qi XM, Qin X, Qu ZY, Räihä T, Rancoita PG, Rapin D, Ricol JS, Rosier-Lees S, Rozhkov A, Rozza D, Sagdeev R, Sandweiss J, Saouter P, Schael S, Schmidt SM, Schulz von Dratzig A, Schwering G, Seo ES, Shan BS, Shi JY, Siedenburg T, Son D, Song JW, Sun WH, Tacconi M, Tang XW, Tang ZC, Tao L, Tescaro D, Ting SCC, Ting SM, Tomassetti N, Torsti J, Türkoğlu C, Urban T, Vagelli V, Valente E, Vannini C, Valtonen E, Vázquez Acosta M, Vecchi M, Velasco M, Vialle JP, Vitale V, Vitillo S, Wang LQ, Wang NH, Wang

QL, Wang X, Wang XQ, Wang ZX, Wei CC, Weng ZL, Whitman K, Wienkenhöver J, Wu H, Wu X, Xia X, Xiong RQ, Xu W, Yan Q, Yang J, Yang M, Yang Y, Yi H, Yu YJ, Yu ZQ, Zeissler S, Zhang C, Zhang J, Zhang JH, Zhang SD, Zhang SW, Zhang Z, Zheng ZM, Zhu ZQ, Zhuang HL, Zhukov V, Zichichi A, Zimmermann N, Zuccon P, AMS Collaboration (2016) Precision measurement of the boron to carbon flux ratio in cosmic rays from 1.9 GV to 2.6 TV with the alpha magnetic spectrometer on the International Space Station. Phys Rev Lett 117(23):231102. https://doi.org/10.1103/PhysRevLett.117.231102

Aguilar M, Ali Cavasonza L, Alpat B, Ambrosi G, Arruda L, Attig N, Aupetit S, Azzarello P, Bachlechner A, Barao F, Barrau A, Barrin L, Bartoloni A, Basara L, Başeğmez-du Pree S, Battarbee M, Battiston R, Becker U, Behlmann M, Beischer B, Berdugo J, Bertucci B, Bindel KF, Bindi V, de Boer W, Bollweg K, Bonnivard V, Borgia B, Boschini MJ, Bourquin M, Bueno EF, Burger J, Cadoux F, Cai XD, Capell M, Caroff S, Casaus J, Castellini G, Cervelli F, Chae MJ, Chang YH, Chen AI, Chen GM, Chen HS, Chen Y, Cheng L, Chou HY, Choumilov E, Choutko V, Chung CH, Clark C, Clavero R, Coignet G, Consolandi C, Contin A, Corti C, Creus W, Crispoltoni M, Cui Z, Dadzie K, Dai YM, Datta A, Delgado C, Della Torre S, Demirköz MB, Derome L, Di Falco S, Dimiccoli F Díaz C, von Doetinchem P, Dong F, Donnini F, Duranti M, D'Urso D, Egorov A, Eline A, Eronen T, Feng J, Fiandrini E, Fisher P, Formato V, Galaktionov Y, Gallucci G, García-López RJ, Gargiulo C, Gast H, Gebauer I, Gervasi M, Ghelfi A, Giovacchini F, Gómez-Coral DM, Gong J, Goy C, Grabski V, Grandi D, Graziani M, Guo KH, Haino S, Han KC, He ZH, Heil M, Hoffman J, Hsieh TH, Huang H, Huang ZC, Huh C, Incagli M, Ionica M, Jang WY, Jia Y, Jinchi H, Kang SC, Kanishev K, Khiali B, Kim GN, Kim KS, Kirn T, Konak C, Kounina O, Kounine A, Koutsenko V, Kulemzin A, La Vacca G, Laudi E, Laurenti G, Lazzizzera I, Lebedev A, Lee HT, Lee SC, Leluc C, Li HS, Li JQ, Li Q, Li TX, Li ZH, Li ZY, Light C, Lim S, Lin CH, Lipari P, Lippert T, Liu D, Liu H, Lordello VD, Lu SQ, Lu YS, Luebelsmeyer K, Luo F, Luo JZ, Luo X, Lyu SS, Machate F, Mañá C, Marín J, Martin T, Martínez G, Masi N, Maurin D, Menchaca-Rocha A, Meng Q, Mikuni VM, Mo DC, Mott P, Nelson T, Ni JQ, Nikonov N, Nozzoli F, Oliva A, Orcinha M, Palermo M, Palmonari F, Palomares C, Paniccia M, Pauluzzi M, Pensotti S, Perrina C, Phan HD, Picot-Clemente N, Pilo F, Pizzolotto C, Plyaskin V, Pohl M, Poireau V, Popkow A, Quadrani L, Qi XM, Qin X, Qu ZY, Räihä T, Rancoita PG, Rapin D, Ricol JS, Rosier-Lees S, Rozhkov A, Rozza D, Sagdeev R, Schael S, Schmidt SM, Schulz von Dratzig A, Schwering G, Seo ES, Shan BS, Shi JY, Siedenburg T, Son D, Song JW, Tacconi M, Tang XW, Tang ZC, Tescaro D, Ting SCC, Ting SM, Tomassetti N, Torsti J, Türkoğlu C, Urban T, Vagelli V, Valente E, Valtonen E, Vázquez Acosta M, Vecchi M, Velasco M, Vialle JP, Wang LQ, Wang NH, Wang QL, Wang X, Wang XQ, Wang ZX, Wei CC, Weng ZL, Whitman K, Wu H, Wu X, Xiong RQ, Xu W, Yan Q, Yang J, Yang M, Yang Y, Yi H, Yu YJ, Yu ZQ, Zannoni M, Zeissler S, Zhang C, Zhang F, Zhang J, Zhang JH, Zhang SW, Zhang Z, Zheng ZM, Zhuang HL, Zhukov V, Zichichi A, Zimmermann N, Zuccon P, AMS Collaboration (2018a) Observation of fine time structures in the cosmic proton and helium fluxes with the alpha magnetic spectrometer on the International Space Station. Phys Rev Lett 121(5):051101. https://doi.org/10.1103/PhysRevLett.121.051101

Aguilar M, Ali Cavasonza L, Ambrosi G, Arruda L, Attig N, Aupetit S, Azzarello P, Bachlechner A, Barao F, Barrau A, Barrin L, Bartoloni A, Basara L, Başeğmez-du Pree S, Battarbee M, Battiston R, Becker U, Behlmann M, Beischer B, Berdugo J, Bertucci B, Bindel KF, Bindi V, de Boer W, Bollweg K, Bonnivard V, Borgia B, Boschini MJ, Bourquin M, Bueno EF, Burger J, Burger WJ, Cadoux F, Cai XD, Capell M, Caroff S, Casaus J, Castellini G, Cervelli F, Chae MJ, Chang YH, Chen AI, Chen GM, Chen HS, Cheng L, Chou HY, Choumilov E, Choutko V, Chung CH, Clark C, Clavero R, Coignet G, Consolandi C, Contin A, Corti C, Creus W, Crispoltoni M, Cui Z, Dadzie K, Dai YM, Datta A, Delgado C, Della Torre S, Demirköz MB, Derome L, Di Falco S, Dimiccoli F Díaz C, von Doetinchem P, Dong F, Donnini F, Duranti M, D'Urso D, Egorov A, Eline A, Eronen T, Feng J, Fiandrini E, Fisher P, Formato V, Galaktionov Y, Gallucci G, García-López RJ, Gargiulo C, Gast H, Gebauer I, Gervasi M, Ghelfi A, Giovacchini F, Gómez-Coral DM, Gong J, Goy C, Grabski V, Grandi D, Graziani M, Guo KH, Haino S, Han KC, He ZH, Heil M, Hsieh TH, Huang H, Huang ZC, Huh C, Incagli M, Ionica M, Jang WY, Jia Y, Jinchi H, Kang SC, Kanishev K, Khiali B, Kim GN, Kim KS, Kirn T, Konak C, Kounina O, Kounine A, Koutsenko V, Kulemzin A, La Vacca G, Laudi E, Laurenti G, Lazzizzera I, Lebedev A, Lee HT, Lee SC, Leluc C, Li HS, Li JQ, Li Q, Li TX, Li Y, Li ZH, Li ZY, Lim S, Lin CH, Lipari P, Lippert T, Liu D, Liu H, Lordello VD, Lu SQ, Lu YS, Luebelsmeyer K, Luo F, Luo JZ, Lyu SS, Machate F, Mañá C, Marín J, Martin T, Martínez G, Masi N, Maurin D, Menchaca-Rocha A, Meng Q, Mikuni VM, Mo DC, Mott P, Nelson T, Ni JQ, Nikonov N, Nozzoli F, Oliva A, Orcinha M, Palermo M, Palmonari F, Palomares C, Paniccia M, Pauluzzi M, Pensotti S, Perrina C, Phan HD, Picot-Clemente N, Pilo F, Pizzolotto C, Plyaskin V, Pohl M, Poireau V, Quadrani L, Qi XM, Qin X, Qu ZY, Räihä T, Rancoita PG, Rapin D, Ricol JS, Rosier-Lees S, Rozhkov A, Rozza D, Sagdeev R, Schael S, Schmidt SM, Schulz von Dratzig A, Schwering G, Seo ES, Shan BS, Shi JY, Siedenburg T, Son D, Song JW, Tacconi M, Tang XW, Tang ZC, Tescaro D, Ting SCC, Ting SM, Tomassetti N, Torsti J, Türkoğlu C, Urban T, Vagelli V, Valente E, Valtonen E, Vázquez Acosta M, Vecchi M, Velasco M, Vialle JP, Vitale V, Wang LQ, Wang NH, Wang

QL, Wang X, Wang XQ, Wang ZX, Wei CC, Weng ZL, Whitman K, Wu H, Wu X, Xiong RQ, Xu W, Yan Q, Yang J, Yang M, Yang Y, Yi H, Yu YJ, Yu ZQ, Zannoni M, Zeissler S, Zhang C, Zhang F, Zhang J, Zhang JH, Zhang SW, Zhang Z, Zheng ZM, Zhuang HL, Zhukov V, Zichichi A, Zimmermann N, Zuccon P, AMS Collaboration (2018b) Observation of new properties of secondary cosmic rays lithium, beryllium, and boron by the alpha magnetic spectrometer on the International Space Station. Phys Rev Lett 120(2):021101. https://doi.org/10.1103/PhysRevLett.120.021101

Aguilar M, Ali Cavasonza L, Ambrosi G, Arruda L, Attig N, Barao F, Barrin L, Bartoloni A, Başeğmez-du Pree S, Bates J, Battiston R, Behlmann M, Beischer B, Berdugo J, Bertucci B, Bindi V, de Boer W, Bollweg K, Borgia B, Boschini MJ, Bourquin M, Bueno EF, Burger J, Burger WJ, Burmeister S, Cai XD, Capell M, Casaus J, Castellini G, Cervelli F, Chang YH, Chen GM, Chen HS, Chen Y, Cheng L, Chou HY, Chouridou S, Choutko V, Chung CH, Clark C, Coignet G, Consolandi C, Contin A, Corti C, Cui Z, Dadzie K, Dai YM, Delgado C, Della Torre S, Demirköz MB, Derome L, Di Falco S, Di Felice V, Díaz C Dimiccoli F, von Doetinchem P, Dong F, Donnini F, Duranti M, Egorov A, Eline A, Feng J, Fiandrini E, Fisher P, Formato V, Freeman C, Galaktionov Y, Gámez C, García-López RJ, Gargiulo C, Gast H, Gebauer I, Gervasi M, Giovacchini F, Gómez-Coral DM, Gong J, Goy C, Grabski V, Grandi D, Graziani M, Guo KH, Haino S, Han KC, Hashmani RK, He ZH, Heber B, Hsieh TH, Hu JY, Huang ZC, Hungerford W, Incagli M, Jang WY, Jia Y, Jinchi H, Kanishev K, Khiali B, Kim GN, Kirn T, Konyushikhin M, Kounina O, Kounine A, Koutsenko V, Kuhlman A, Kulemzin A, La Vacca G, Laudi E, Laurenti G, Lazzizzera I, Lebedev A, Lee HT, Lee SC, Leluc C, Li JQ, Li M, Li Q, Li S, Li TX, Li ZH, Light C, Lin CH, Lippert T, Liu Z, Lu SQ, Lu YS, Luebelsmeyer K, Luo JZ, Lyu SS, Machate F, Mañá C, Marín J, Marquardt J, Martin T, Martínez G, Masi N, Maurin D, Menchaca-Rocha A, Meng Q, Mo DC, Molero M, Mott P, Mussolin L, Ni JQ, Nikonov N, Nozzoli F, Oliva A, Orcinha M, Palermo M, Palmonari F, Paniccia M, Pashnin A, Pauluzzi M, Pensotti S, Phan HD, Plyaskin V, Pohl M, Porter S, Qi XM, Qin X, Qu ZY, Quadrani L, Rancoita PG, Rapin D, Reina Conde A, Rosier-Lees S, Rozhkov A, Rozza D, Sagdeev R, Schael S, Schmidt SM, Schulz von Dratzig A, Schwering G, Seo ES, Shan BS, Shi JY, Siedenburg T, Solano C, Song JW, Sonnabend R, Sun Q, Sun ZT, Tacconi M, Tang XW, Tang ZC, Tian J, Ting SCC, Ting SM, Tomassetti N, Torsti J, Tüysüz C, Urban T, Usoskin I, Vagelli V, Vainio R, Valente E, Valtonen E, Vázquez Acosta M, Vecchi M, Velasco M, Vialle JP, Wang LQ, Wang NH, Wang QL, Wang S, Wang X, Wang ZX, Wei J, Weng ZL, Wu H, Xiong RQ, Xu W, Yan Q, Yang Y, Yi H, Yu YJ, Yu ZQ, Zannoni M, Zhang C, Zhang F, Zhang FZ, Zhang JH, Zhang Z, Zhao F, Zheng ZM, Zhuang HL, Zhukov V, Zichichi A, Zimmermann N, Zuccon P (2021) The Alpha Magnetic Spectrometer (AMS) on the International Space Station: part II – results from the first seven years. Phys Rep 894:1–116. https://doi.org/10.1016/j.physrep.2020.09.003.

Akhoondzadeh M, Parrot M, Saradjian MR (2010) Electron and ion density variations before strong earthquakes (M > 6.0) using DEMETER and GPS data. Nat Hazards Earth Syst Sci 10(1):7–18. https://doi.org/10.5194/nhess-10-7-2010

Aleksandrin SY, Galper AM, Grishantzeva LA, Koldashov SV, Maslennikov LV, Murashov AM, Picozza P, Sgrigna V, Voronov SA (2003) High-energy charged particle bursts in the near-Earth space as earthquake precursors. Ann Geophys 21(2):597–602. https://doi.org/10.5194/angeo-21-597-2003

Ambrosi G, Bartocci S, Basara L, Battiston R, Burger WJ, Campana D, Carfora L, Castellini G, Cipollone P, Conti L, Contin A, De Donato C, De Persio F, De Santis C, Follega FM, Guandalini C, Ionica M, Iuppa R, Laurenti G, Lazzizzera I, Lolli M, Manea C, Martucci M, Masciantonio G, Mergé M, Osteria G, Pacini L, Palma F, Palmonari F, Panico B, Parmentier A, Patrizii L, Perfetto F, Picozza P, Piersanti M, Pozzato M, Puel M, Rashevskaya I, Ricci E, Ricci M, Ricciarini S, Scotti V, Sotgiu A, Sparvoli R, Spataro B, Vitale V, Zoffoli S, Zuccon P (2020) Beam test calibrations of the HEPD detector on board the China seismo-electromagnetic satellite. Nucl Instrum Methods Phys Res, Sect A, Accel Spectrom Detect Assoc Equip 974:164170. https://doi.org/10.1016/j.nima.2020.164170

Ambrosi G, Bartocci S, Basara L, Battiston R, Burger WJ, Campana D, Caprai M, Carfora L, Castellini G, Cipollone P, Conti L, Contin A, De Donato C, De Persio F, De Santis C, Follega FM, Guandalini C, Gebbia G, Ionica M, Iuppa R, Laurenti G, Lazzizzera I, Lolli M, Manea C, Martucci M, Masciantonio G, Mergè M, Mese M, Osteria G, Pacini L, Palma F, Palmonari F, Panico B, Parmentier A, Patrizii L, Perfetto F, Picozza P, Pozzato M, Puel M, Rashevskaya I, Ricci E, Ricci M, Ricciarini S, Sahnoun Z, Scotti V, Sotgiu A, Sparvoli R, Vitale V, Zoffoli S, Zuccon P (2021) The electronics of the high-energy particle detector on board the CSES-01 satellite. Nucl Instrum Methods Phys Res, Sect A, Accel Spectrom Detect Assoc Equip 1013:165639. https://doi.org/10.1016/j.nima.2021.165639

Anastasio A, Bartocci S, Battiston R, Beolè S, Benotto F, Boiano A, Cipollone P, Coli S, Contin A, Cristoforetti M, De Donato C, De Santis C, Di Luca A, Dumitrache F, Follega FM, Garrafa Botta S, Gebbia G, Iuppa R, Lega A, Lolli M, Masciantonio G, Masone V, Mergè M, Mese M, Nicolaidis R, Nozzoli F, Oliva A, Osteria G, Palma F, Palmonari F, Panico B, Perciballi S, Perfetto F, Picozza P, Pozzato M, Ricci E, Ricci M, Ricciarini SB, Sahnoun Z, Savino U, Scotti V, Serra E, Sotgiu A, Sparvoli R, Ubertini P, Vanzanella A, Vilona V, Zoffoli S, Zuccon P (2025) Trigger and calorimeter data acquisition of the

High-Energy Particle Detector onboard the CSES-02 satellite. IEEE Trans Instrum Meas, 1–1. https://doi.org/10.1109/TIM.2025.3555671

Aschwanden MJ (2012) GeV particle acceleration in solar flares and Ground Level Enhancement (GLE) events. Space Sci Rev 171(1–4):3–21. https://doi.org/10.1007/s11214-011-9865-x

Astafyeva E, Yasyukevich YV, Maletckii B, Oinats A, Vesnin A, Yasyukevich AS, Syrovatskii S, Guendouz N (2022) Ionospheric Disturbances and Irregularities During the 25–26 August 2018 Geomagnetic Storm. J Geophys Res Space Phys 127(1). https://doi.org/10.1029/2021JA029843

Bakaldin AV, Batishchev AG, Voronov SA, Galper AM, Grishantseva LA, Koldashov SV, Naumov PY, Chesnokov VY, Shilov VA (2007) Satellite experiment ARINA for studying seismic effects in the high-energy particle fluxes in the Earth's magnetosphere. Cosm Res 45(5):445–448. https://doi.org/10.1134/S0010952507050085

Baker DN (2021) Wave–particle interaction effects in the Van Allen belts. Earth Planets Space 73(1). https://doi.org/10.1186/s40623-021-01508-y

Baker DN, Mason GM, Hamilton DC, Rosenvinge TT, Blake JB, Callis LB, Hovestadt D, Klecker B, Scholer M, Mewaldt RA (1993) An overview of the Solar, Anomalous, and Magnetospheric Particle Explorer (SAMPEX) mission. IEEE Trans Geosci Remote Sens 31(3):606–614. https://doi.org/10.1109/36.206267

Barioglio L, Bartocci S, Battiston R, Beolè S, Benotto F, Bufalino S, Cipollone P, Coli S, Contin A, Cristoforetti M, De Donato C, De Santis C, Di Luca A, Dumitrache F, Ferrero C, Follega FM, Garrafa Botta S, Gebbia G, Iuppa R, Lega A, Lolli M, Masciantonio G, Mergè M, Mese M, Nicolaidis R, Nozzoli F, Oliva A, Osteria G, Palma F, Palmonari F, Panico B, Perciballi S, Perfetto F, Picozza P, Pozzato M, Ricci M, Ricci E, Ricciarini SB, Sahnoun Z, Savino U, Scotti V, Serra E, Sotgiu A, Sparvoli R, Ubertini P, Vilona V, Zoffoli S, Zuccon P (2025) The Monolithic Active Pixel Sensors Tracker System of the High Energy Particle Detector aboard the Second Chinese Seismo-Electromagnetic Satellite. IEEE Aerosp Electron Syst Mag, 1–16. https://doi.org/10.1109/MAES.2025.3568361

Barthelmy SD, Barbier LM, Cummings JR, Fenimore EE, Gehrels N, Hullinger D, Krimm HA, Markwardt CB, Palmer DM, Parsons A, Sato G, Suzuki M, Takahashi T, Tashiro M, Tueller J (2005) The Burst Alert Telescope (BAT) on the SWIFT Midex Mission. Space Sci Rev 120(3–4):143–164. https://doi.org/10.1007/s11214-005-5096-3

Bartocci S, Battiston R, Burger WJ, Campana D, Carfora L, Castellini G, Conti L, Contin A, De Donato C, De Persio F, De Santis C, Diego P, Follega FM, Iuppa R, Lazzizzera I, Marcelli N, Martucci M, Masciantonio G, Mergè M, Osteria G, Palma F, Palmonari F, Parmentier A, Perfetto F, Picozza P, Piersanti M, Pozzato M, Rashevskaya I, Ricci E, Ricci M, Ricciarini S, Scotti V, Sotgiu A, Sparvoli R, Ubertini P, Vitale V, Zoffoli S, Zuccon P (2020) Galactic cosmic-ray hydrogen spectra in the 40–250 MeV range measured by the High-Energy Particle Detector (HEPD) on board the CSES-01 satellite between 2018 and 2020. Astrophys J 901(1):8. https://doi.org/10.3847/1538-4357/abad3e

Bartocci S, Battiston R, Benotto F, Beolè S, Burger WJ, Campana D, Castellini G, Cipollone P, Coli S, Conti L, Contin A, Cristoforetti M, De Cilladi L, De Donato C, De Santis C, Follega FM, Gebbia G, Iuppa R, Lolli M, Marcelli N, Martucci M, Masciantonio G, Mergè M, Mese M, Neubüser C, Nozzoli F, Oliva A, Osteria G, Pacini L, Palma F, Palmonari F, Parmentier A, Perfetto F, Picozza P, Piersanti M, Pozzato M, Ricci E, Ricci M, Ricciarini SB, Sahnoun Z, Scotti V, Sotgiu A, Sparvoli R, Vitale V, Zoffoli S, Zuccon P (2022) Deep learning based event reconstruction for the limadou high-energy particle detector. Phys Rev D 105:022004. https://doi.org/10.1103/PhysRevD.105.022004

Bartocci S, Battiston R, Benella S, Beolè S, Burger WJ, Cipollone P, Contin A, Cristoforetti M, De Donato C, De Santis C, Di Luca A, Follega FM, Gebbia G, Iuppa R, Laurenza M, Lega A, Lolli M, Martucci M, Masciantonio G, Mergè M, Mese M, Neubuser C, Nicolaidis R, Nozzoli F, Oliva A, Osteria G, Palma F, Panico B, Perfetto F, Perinelli A, Picozza P, Ricci E, Ricci M, Ricciarini SB, Sahnoun Z, Savino U, Scotti V, Sorbara M, Sotgiu A, Sparvoli R, Ubertini P, Vilona V, Zoffoli S, Zuccon P (2024a) Multispacecraft observations of protons and helium nuclei in some solar energetic particle events toward the maximum of cycle 25. Astrophys J 974(2):176. https://doi.org/10.3847/1538-4357/ad7395

Bartocci S, Battiston R, Beolè S, Benotto F, Cipollone P, Coli S, Contin A, Cristoforetti M, De Donato C, De Santis C, Di Luca A, Dumitrache F, Follega FM, Garrafa Botta S, Gebbia G, Iuppa R, Lega A, Lolli M, Masciantonio G, Mergè M, Mese M, Nicolaidis R, Nozzoli F, Oliva A, Osteria G, Palma F, Palmonari F, Panico B, Perciballi S, Perfetto F, Picozza P, Pozzato M, Ricci E, Ricci M, Ricciarini SB, Sahnoun Z, Savino U, Scotti V, Serra E, Sotgiu A, Sparvoli R, Ubertini P, Vilona V, Zoffoli S, Zuccon P (2024c) The scintillation counters of the high-energy particle detector of the China Seismo-Electromagnetic (CSES-02) satellite. Remote Sens 16(21):3982. https://doi.org/10.3390/rs16213982

Bartocci S, Battiston R, Beolè S, Burger WJ, Campana D, Cipollone P, Contin A, Cristoforetti M, De Donato C, De Santis C, Di Luca A, Follega FM, Gebbia G, Iuppa R, Lega A, Lolli M, Martucci M, Masciantonio G, Mergè M, Mese M, Neubüser C, Nicolaidis R, Nozzoli F, Oliva A, Osteria G, Palma F, Panico B, Perfetto F, Perinelli A, Picozza P, Ricci E, Ricci L, Ricci M, Ricciarini SB, Sahnoun Z, Savino U, Scotti

V, Sorbara M, Sotgiu A, Sparvoli R, Ubertini P, Vilona V, Zoffoli S, Zuccon P (2024b) The catalogue of gamma-ray burst observations by HEPD-01 in the 0.3–50 MeV energy range. Astrophys J 976(2):239. https://doi.org/10.3847/1538-4357/ad822c

Bartocci S, Battiston R, Beolè S, Benotto F, Castellini G, Cipollone P, Coli S, Contin A, Cristoforetti M, De Donato C, De Santis C, Di Luca A, Dumitrache F, Follega FM, Garrafa Botta S, Gebbia G, Iuppa R, Lega A, Lolli M, Masciantonio G, Mergè M, Mese M, Nicolaidis R, Nozzoli F, Oliva A, Osteria G, Palma F, Palmonari F, Panico B, Perciballi S, Perfetto F, Picozza P, Pozzato M, Ricci E, Ricci M, Ricciarini SB, Sahnoun Z, Savino U, Scotti V, Serra E, Sotgiu A, Sparvoli R, Ubertini P, Vilona V, Zoffoli S, Zuccon P (2025a) Development of the power supply of HEPD-02 instrument on board CSES-02 satellite. J Instrum 20(06):06005. https://doi.org/10.1088/1748-0221/20/06/P06005

Bartocci S, Battiston R, Beolè S, Benotto F, Cipollone P, Coli S, Contin A, Cristoforetti M, De Donato C, De Santis C, Dumitrache F, Di Luca A, Follega FM, Garrafa Botta S, Gebbia G, Iuppa R, Lega A, Lolli M, Masciantonio G, Mergè M, Mese M, Nicolaidis R, Nozzoli F, Oliva A, Osteria G, Palma F, Palmonari F, Panico B, Perciballi S, Perfetto F, Picozza P, Pozzato M, Ricci M, Ricci E, Ricciarini SB, Sahnoun Z, Savino U, Scotti V, Serra E, Sotgiu A, Sparvoli R, Ubertini P, Vilona V, Zoffoli S, Zuccon P (2025c) TROPix: a parametric tool reproducing the output of the HEPD-02 pixel detector. Nucl Instrum Methods Phys Res, Sect A, Accel Spectrom Detect Assoc Equip 1080:170756. https://doi.org/10.1016/j.nima.2025.170756

Bartocci S, Battiston R, Beolè S, Burger WJ, Campana D, Cipollone P, Contin A, Cristoforetti M, De Donato C, De Santis C, Di Luca A, Follega FM, Gebbia G, Iuppa R, Lega A, Lolli M, Martucci M, Masciantonio G, Mergè M, Mese M, Neubüser C, Nicolaidis R, Nozzoli F, Oliva A, Osteria G, Palma F, Panico B, Perfetto F, Perinelli A, Picozza P, Ricci E, Ricci L, Ricci M, Ricciarini SB, Sahnoun Z, Savino U, Scotti V, Sorbara M, Sotgiu A, Sparvoli R, Ubertini P, Vilona V, Zoffoli S, Zuccon P (2025b) Mapping the South Atlantic Anomaly charged particle environment with the HEPD-01 detector on board the CSES-01 satellite. Phys Rev D 111:022001. https://doi.org/10.1103/PhysRevD.111.022001

Battiston R, Vitale V (2013) First evidence for correlations between electron fluxes measured by NOAA-POES satellites and large seismic events. Nucl Phys B, Proc Suppl 243–244:249–257. https://doi.org/10.1016/j.nuclphysbps.2013.09.002. Proceedings of the IV International Conference on Particle and Fundamental Physics in Space

Battiston R, Neubüser C, Follega FM, Iuppa R, Vitale V, Ammendola R, Badoni D, Bartocci S, Bazzano A, Beolè S, Bertello I, Burger WJ, Campana D, Cicone A, Cipollone P, Coli S, Conti L, Contin A, Cristoforetti M, D'Angelo G, De Angelis F, De Donato C, De Santis C, Diego P, Di Luca A, Fiorenza E, Gebbia G, Lega A, Lolli M, Martino B, Martucci M, Masciantonio G, Mergè M, Mese M, Morbidini A, Nuccilli F, Nozzoli F, Oliva A, Osteria G, Papini E, Palma F, Palmonari F, Parmentier A, Panico B, Perciballi S, Perfetto F, Perinelli A, Picozza P, Piersanti M, Pozzato M, Rebustini G, Recchiuti D, Ricci E, Ricci M, Rodi J, Russi A, Ricciarini SB, Sahnoun Z, Savino U, Scotti V, Shen X, Sotgiu A, Sparvoli R, Tofani S, Ubertini P, Vertolli N, Vilona V, Zannoni U, Zeren Z, Zoffoli S, Zuccon P (2023) Observation of anomalous electron fluxes induced by GRB221009A on CSES-01 low-energy charged particle detector. Astrophys J Lett 946(1):29. https://doi.org/10.3847/2041-8213/acc247

Belov AV, Eroshenko EA, Oleneva VA, Struminsky AB, Yanke VG (2001) What determines the magnitude of forbush decreases? Adv Space Res 27(3):625–630. https://doi.org/10.1016/S0273-1177(01)00095-3

Berrilli F, Casolino M, Del Moro D, Di Fino L, Larosa M, Narici L, Piazzesi R, Picozza P, Scardigli S, Sparvoli R, Stangalini M, Zaconte V (2014) The relativistic solar particle event of May 17th, 2012 observed on board the International Space Station. J Space Weather Space Clim 4:16. https://doi.org/10.1051/swsc/2014014

Berthelier JJ, Godefroy M, Leblanc F, Malingre M, Menvielle M, Lagoutte D, Brochot JY, Colin F, Elie F, Legendre C, Zamora P, Benoist D, Chapuis Y, Artru J, Pfaff R (2006) ICE, the electric field experiment on DEMETER. Planet Space Sci 54(5):456–471. https://doi.org/10.1016/j.pss.2005.10.016

Bortnik J, Thorne RM (2007) The dual role of ELF/VLF chorus waves in the acceleration and precipitation of radiation belt electrons. J Atmos Sol-Terr Phys 69(3):378–386. https://doi.org/10.1016/j.jastp.2006.05.030. Global Aspects of Magnetosphere-Ionosphere Coupling

Boschini MJ, Della Torre S, Gervasi M, La Vacca G, Rancoita PG (2022) The transport of galactic cosmic rays in heliosphere: the HelMod model compared with other commonly employed solar modulation models. Adv Space Res 70(9):2636–2648. https://doi.org/10.1016/j.asr.2022.03.026. Astrophysics of Cosmic Rays

Bragg WH (1904) LXXIII. On the absorption of α rays, and on the classification of the α rays from radium. Lond Edinb Dublin Philos Mag J Sci 8(48):719–725. https://doi.org/10.1080/14786440409463245

Bruno R, Carbone V (2013) The solar wind as a turbulence laboratory. Living Rev Sol Phys 10:2. https://doi.org/10.12942/lrsp-2013-2

Bruno A, Bazilevskaya GA, Boezio M, Christian ER, De Nolfo GA, Martucci M, Mergè M, Mikhailov VV, Munini R, Richardson IG, Ryan JM, Stochaj S, Adriani O, Barbarino GC, Bellotti R, Bogomolov EA,

Bongi M, Bonvicini V, Bottai S, Cafagna F, Campana D, Carlson P, Casolino M, Castellini G, De Santis C, Di Felice V, Galper AM, Karelin AV, Koldashov SV, Koldobskiy S, Krutkov SY, Kvashnin AN, Leonov A, Malakhov V, Marcelli L, Mayorov AG, Menn W, Mocchiutti E, Monaco A, Mori N, Osteria G, Panico B, Papini P, Pearce M, Picozza P, Ricci M, Ricciarini SB, Simon M, Sparvoli R, Spillantini P, Stozhkov YI, Vacchi A, Vannuccini E, Vasilyev GI, Voronov SA, Yurkin YT, Zampa G, Zampa N (2018) Solar energetic particle events observed by the PAMELA mission. Astrophys J 862(2):97. https://doi.org/10.3847/1538-4357/aacc26

Bruno A, Martucci M, Cafagna FS, Sparvoli R, Adriani O, Barbarino GC, Bazilevskaya GA, Bellotti R, Boezio M, Bogomolov EA, Bongi M, Bonvicini V, Campana D, Carlson P, Casolino M, Castellini G, De Santis C, Galper AM, Koldashov SV, Koldobskiy S, Kvashnin AN, Lenni A, Leonov AA, Malakhov VV, Marcelli L, Marcelli N, Mayorov AG, Menn W, Mergè M, Mocchiutti E, Monaco A, Mori N, Mikhailov VV, Munini R, Osteria G, Panico B, Papini P, Pearce M, Picozza P, Ricci M, Ricciarini SB, Simon M, Sotgiu A, Spillantini P, Stozhkov YI, Vacchi A, Vannuccini E, Vasilyev GI, Voronov SA, Yurkin YT, Zampa G, Zampa N, Zharaspayev TR (2021) Solar-cycle variations of South Atlantic Anomaly proton intensities measured with the PAMELA mission. Astrophys J Lett 917(2):21. https://doi.org/10.3847/2041-8213/ac1a74

Burch JL, Torbert RB, Phan TD, Chen L-J, Moore TE, Ergun RE, Eastwood JP, Gershman DJ, Hesse M, Cassak PA, Argall MR, Gershman DJ (2016) Magnetospheric Multiscale overview and science objectives. Space Sci Rev 199:5–21. https://doi.org/10.1007/s11214-015-0164-9

Cane HV (2000) Coronal mass ejections and Forbush decreases. Space Sci Rev 93:55–77. https://doi.org/10.1023/A:1026532125747

Carbone V, Piersanti M, Materassi M, Battiston R, Lepreti F, Ubertini P (2021) A mathematical model of lithosphere–atmosphere coupling for seismic events. Sci Rep 11(1):8682. https://doi.org/10.1038/s41598-021-88125-7

Chenette DL, Conlon TF, Pyle KR, Simpson JA (1977) Observations of Jovian electrons at 1 AU throughout the 13-month Jovian synodic year. Astrophys J 211:954–959. https://doi.org/10.1086/182487

Chytracek R, Mccormick J, Pokorski W, Santin G (2006) Geometry description markup language for physics simulation and analysis applications. IEEE Trans Nucl Sci 53(5):2892–2896. https://doi.org/10.1109/TNS.2006.881062

Coli S, Angeletti M, Gargiulo C, Iuppa R, Serra E (2022) Thermo-mechanical design for ALPIDE pixel sensor chip in a high-energy particle detector space module. J Instrum 17(01):01019. https://doi.org/10.1088/1748-0221/17/01/C01019

Bartocci S, Battiston R, Beolè S, Benotto F, Cipollone P, Coli S, Contin A, Cristoforetti M, De Donato C, De Santis C, Di Luca A, Dumitrache F, Follega FM, Garrafa Botta S, Gebbia G, Iuppa R, Lega A, Lolli M, Masciantonio G, Mergè M, Mese M, Nicolaidis R, Nozzoli F, Oliva A, Osteria G, Palma F, Palmonari F, Panico B, Perciballi S, Perfetto F, Picozza P, Pozzato M, Ricci E, Ricci M, Ricciarini SB, Sahnoun Z, Savino U, Scotti V, Serra E, Sotgiu A, Sparvoli R, Ubertini P, Vilona V, Zoffoli S, Zuccon P (2026) Control and read-out of the HEPD-02 tracking system onboard CSES-02 satellite. J Instrum 21(01):01030. https://doi.org/10.1088/1748-0221/21/01/P01030

Bartocci S, Battiston R, Beolè S, Benotto F, Cipollone P, Coli S, Contin A, Cristoforetti M, De Donato C, De Santis C, Di Luca A, Dumitrache F, Follega FM, Garrafa Botta S, Gebbia G, Iuppa R, Lega A, Lolli M, Masciantonio G, Mergè M, Mese M, Nicolaidis R, Nozzoli F, Oliva A, Osteria G, Palma F, Palmonari F, Panico B, Perciballi S, Perfetto F, Picozza P, Pozzato M, Ricci E, Ricci M, Ricciarini SB, Sahnoun Z, Savino U, Scotti V, Serra E, Sotgiu A, Sparvoli R, Ubertini P, Vilona V, Zoffoli S, Zuccon P (2026) Critical Aspects in the Modelling of Sub-GeV Calorimetric Particle Detectors: The Case Study of the High-Energy Particle Detector (HEPD-02) on Board the CSES-02 Satellite. Particles 9(1):6. https://doi.org/10.3390/particles9010006

Damiani A, Storini M, Laurenza M, Rafanelli C (2008) Solar particle effects on minor components of the polar atmosphere. Ann Geophys 26(2):361–370. https://doi.org/10.5194/angeo-26-361-2008

Di Giulio C, Buonomo B, Cardelli F, Di Giovenale D, Foggetta L, Moriggi D (2022) The Frascati DAΦNE LINAC and the Beam Test Facility (BTF) Setups for Irradiation. JACoW IPAC2022" 010. https://doi.org/10.18429/JACoW-IPAC2022-THPOST010

Diego P, Badoni D, De Santis C, Papini E, Parmentier A, Piersanti M, Conti L, Rebustini G, Ammendola R, Bartocci S, Battiston R, Bertello I, Cipollone P, D'Angelo G, De Angelis F, Fiorenza E, Masciantonio G, Morbidini A, Nuccilli F, Picozza P, Russi A, Sotgiu A, Sparvoli R, Tofani S, Ubertini P, Vertolli N, Zannoni U, Zoffoli S (2025) Electric field detector on board the CSES-02 satellite for characterization of ionospheric plasma dynamics. Space Sci Rev 221(3):39. https://doi.org/10.1007/s11214-025-01167-5

EJ200 (2021) General purpose EJ-200, EJ-204. EJ-208, EJ-212. https://eljentechnology.com/products/plastic-scintillators/ej-200-ej-204-ej-208-ej-212. Accessed: 2021-08-04

Escoubet CP, Fehringer M, Goldstein M (2001) Introduction: the cluster mission. Ann Geophys 19(10/12):1197–1200. https://doi.org/10.5194/angeo-19-1197-2001

Evenson P, Meyer P (1983) Solar modulation of cosmic-ray electrons 1978–1983. Int Cosm Ray Conf 3:31
Fidani C, Battiston R, Burger WJ (2010) A study of the correlation between earthquakes and NOAA satellite energetic particle bursts. Remote Sens 2(9):2170–2184. https://doi.org/10.3390/rs2092170
Force USS (1962) Defense Meteorological Satellite Program (DMSP). U.S. Air Force / U.S. Space Force – environmental 'I&' space-weather satellite program. Deployed since August 1962; provides global meteorological, oceanographic, and space environment observations via a constellation of near-polar, sun-synchronous satellites. https://www.spaceforce.mil/About-Us/Fact-Sheets/Defense-Meteorological-Satellite-Program/
Gabici S (2022) Low-energy cosmic rays: regulators of the dense interstellar medium. Astron Astrophys Rev 30(1):4. https://doi.org/10.1007/s00159-022-00141-2
Giacalone J, Fahr H, Fichtner H, Florinski V, Heber B, Hill ME, Kóta J, Leske RA, Potgieter MS, Rankin JS (2022) Anomalous cosmic rays and heliospheric energetic particles. Space Sci Rev 218(4):22. https://doi.org/10.1007/s11214-022-00890-7
Giesen G, Boudaud M, Génolini Y, Poulin V, Cirelli M, Salati P, Serpico PD (2015) AMS-02 antiprotons, at last! Secondary astrophysical component and immediate implications for dark matter. J Cosmol Astropart Phys 2015(09):023. https://doi.org/10.1088/1475-7516/2015/09/023
Ginet GP, O'Brien TP, Huston SL, Johnston WR, Guild TB, Friedel R, Lindstrom CD, Roth CJ, Whelan P, Quinn RA, Madden D, Morley S, Su Y-J (2013) AE9, AP9 and SPM: new models for specifying the trapped energetic particle and space plasma environment. Space Sci Rev 179:579–615. https://doi.org/10.1007/s11214-013-9964-y
Gusev AA, Pugacheva GI, Jayanthi UB, Schuch N (2003) Modeling of low-altitude quasi-trapped proton fluxes at the equatorial inner magnetosphere. Braz J Phys 33(4):775–781. https://doi.org/10.1590/s0103-97332003000400029
Harrison RG, Aplin KL, Rycroft MJ (2010) Atmospheric electricity coupling between earthquake regions and the ionosphere. J Atmos Sol-Terr Phys 72(5–6):376–381. https://doi.org/10.1016/j.jastp.2009.12.004
Huttunen-Heikinmaa K, Valtonen E, Laitinen T (2005) Proton and helium release times in SEP events observed with SOHO/ERNE. Astron Astrophys 442(2):673–685. https://doi.org/10.1051/0004-6361:20042620
Jackman CH, Deland MT, Labow GJ, Fleming EL, Weisenstein DK, Ko MKW, Sinnhuber M, Russell JM (2005) Neutral atmospheric influences of the solar proton events in October-November 2003. J Geophys Res Space Phys 110(A9):09. https://doi.org/10.1029/2004JA010888
Kaladze TD, Pokhotelov OA, Shah HA, Khan MI, Stenflo L (2008) Acoustic-gravity waves in the Earth's ionosphere. J Atmos Sol-Terr Phys 70(13):1607–1616. https://doi.org/10.1016/j.jastp.2008.06.009
Kintner PM, Ledvina BM, de Paula ER (2007) GPS and ionospheric scintillations. Space Weather 5(9). https://doi.org/10.1029/2006SW000260
Korsmeier M, Donato F, Fornengo N (2018) Prospects to verify a possible dark matter hint in cosmic antiprotons with antideuterons and antihelium. Phys Rev D 97:103011. https://doi.org/10.1103/PhysRevD.97.103011
Kotzé P (2023) Behaviour of 27-day and 13.5-day periodicities in galactic cosmic particles as observed by spacecraft and neutron monitors during different solar polarity cycles. Sophia Perennis 298(9):107. https://doi.org/10.1007/s11207-023-02203-9
Kusnierkiewicz DY (2003) An overview of the TIMED spacecraft. Johns Hopkins APL Tech Dig 24(2):147–155
Leer E, Holzer TE, Flå T (1982) Acceleration of the solar wind. Space Sci Rev 33(1):161–200. https://doi.org/10.1007/BF00213253
Li XQ, Xu YB, An ZH, Liang XH, Wang P, Zhao XY, Wang HY, Lu H, Ma YQ, Shen XH, Wen XY, Wang H, Zhang DL, Shi F, Peng WX, Gao M, Yu XX, Wang JZ, Zhang YJ, Zhang JL, Zhang J, Li HX, Zeng JR, Nan YF (2019) The high-energy particle package onboard CSES. Radiat Detect Technol Methods 3(3):22. https://doi.org/10.1007/s41605-019-0101-7
Liu L, Wan W, Chen Y, Le H (2011) Solar activity effects of the ionosphere: a brief review. Chin Sci Bull 56(12):1202–1211. https://doi.org/10.1007/s11434-010-4226-9
Lockwood JA (1971) Forbush decreases in the cosmic radiation. Space Sci Rev 12(5):658–715. https://doi.org/10.1007/BF00173346
Macmillan S, Olsen N (2013) Observatory data and the Swarm mission. Earth Planets Space 65:1355–1362. https://doi.org/10.5047/eps.2013.07.011
Martucci M, Sparvoli R, Bartocci S, Battiston R, Burger WJ, Campana D, Carfora L, Castellini G, Conti L, Contin A, De Donato C, De Santis C, Follega FM, Iuppa R, Lazzizzera I, Marcelli N, Masciantonio G, Mergè M, Oliva A, Osteria G, Palma F, Palmonari F, Panico B, Parmentier A, Perfetto F, Picozza P, Piersanti M, Pozzato M, Ricci E, Ricci M, Ricciarini SB, Sahnoun Z, Scotti V, Sotgiu A, Vitale V, Zoffoli S, Zuccon P (2021) Trapped Proton Fluxes Estimation Inside the South Atlantic Anomaly Using

the NASA AE9/AP9/SPM Radiation Models along the China Seismo-Electromagnetic Satellite Orbit. Appl Sci 11(8):3465. https://doi.org/10.3390/app11083465

Martucci M, Bartocci S, Battiston R, Campana D, Carfora L, Conti L, Contin A, De Donato C, De Santis C, Follega FM, Iuppa R, Marcelli N, Masciantonio G, Mergè M, Oliva A, Osteria G, Palma F, Parmentier A, Perfetto F, Picozza P, Pozzato M, Ricci E, Ricci M, Ricciarini SB, Sahnoun Z, Scotti V, Sotgiu A, Sparvoli R, Vitale V, Zoffoli S, Zuccon P (2022) New results on protons inside the South Atlantic Anomaly, at energies between 40-250 MeV in the period 2018-2020, from the CSES-01 satellite mission. Phys Rev D 105:062001. https://doi.org/10.1103/PhysRevD.105.062001

Martucci M, Ammendola R, Badoni D, Bartocci S, Battiston R, Beolè S, Burger WJ, Campana D, Castellini G, Cipollone P, Coli S, Conti L, Contin A, Cristoforetti M, D'Angelo G, De Donato C, De Santis C, Di Luca A, Follega FM, Gebbia G, Iuppa R, Lega A, Lolli M, Marcelli N, Masciantonio G, Mergè M, Mese M, Neubüser C, Nozzoli F, Oliva A, Osteria G, Pacini L, Palma F, Palmonari F, Panico B, Parmentier A, Perciballi S, Perfetto F, Picozza P, Pozzato M, Rebustini GM, Ricci E, Ricci M, Ricciarini SB, Savino U, Sahnoun Z, Scotti V, Sotgiu A, Sparvoli R, Ubertini P, Vilona V, Vitale V, Zoffoli S, Zuccon P, Aslam OPM, Ngobeni MD, Potgieter MS (2023a) Time dependence of 50-250 MeV galactic cosmic-ray protons between solar cycles 24 and 25, measured by the high-energy particle detector on board the CSES-01 satellite. Astrophys J Lett 945(2):39. https://doi.org/10.3847/2041-8213/acbea7

Martucci M, Laurenza M, Benella S, Berrilli F, Del Moro D, Giovannelli L, Parmentier A, Piersanti M, Albrecht G, Bartocci S, Battiston R, Burger WJ, Campana D, Carfora L, Consolini G, Conti L, Contin A, De Donato C, De Santis C, Follega FM, Iuppa R, Lega A, Marcelli N, Masciantonio G, Mergè M, Mese M, Oliva A, Osteria G, Palma F, Panico B, Perfetto F, Picozza P, Pozzato M, Ricci E, Ricci M, Ricciarini SB, Sahnoun Z, Scotti V, Sotgiu A, Sparvoli R, Vitale V, Zoffoli S, Zuccon P (2023b) The first ground-level enhancement of solar cycle 25 as seen by the High-Energy Particle Detector (HEPD-01) on board the CSES-01 satellite. Space Weather 21(1):2022–003191. https://doi.org/10.1029/2022SW003191

Martucci M, Oliva A, Battiston R, Beolè S, Cipollone P, Contin A, Cristoforetti M, De Donato C, De Santis C, Di Luca A, Follega FM, Gebbia G, Iuppa R, Lega A, Lolli M, Masciantonio G, Mese M, Neubuser C, Nicolaidis R, Nozzoli F, Osteria G, Palma F, Panico B, Perfetto F, Perinelli A, Picozza P, Ricci E, Ricci M, Ricciarini SB, Sahnoun Z, Savino U, Scotti V, Sorbara M, Sotgiu A, Sparvoli R, Ubertini P, Vilona V, Zoffoli S, Zuccon P (2024) Measurements of low-energy, re-entrant albedo protons by the HEPD-01 space-borne detector. Astropart Phys 162:102993. https://doi.org/10.1016/j.astropartphys.2024.102993

Mechbal S, Mangeard P-S, Clem JM, Evenson PA, Johnson RP, Lucas B, Roth J (2020) Measurement of low-energy cosmic-ray electron and positron spectra at 1 au with the AESOP-lite spectrometer. Astrophys J 903(1):21. https://doi.org/10.3847/1538-4357/abb46f

Meegan C, Lichti G, Bhat PN, Bissaldi E, Briggs MS, Connaughton V, Diehl R, Fishman G, Greiner J, Hoover AS, van der Horst AJ, von Kienlin A, Kippen RM, Kouveliotou C, McBreen S, Paciesas WS, Preece R, Steinle H, Wallace MS, Wilson RB, Wilson-Hodge C (2009) The Fermi Gamma-Ray Burst monito. Astrophys J 702(1):791. https://doi.org/10.1088/0004-637X/702/1/791

Mewaldt RA, Cohen CMS, Labrador AW, Leske RA, Mason GM, Desai MI, Looper MD, Mazur JE, Selesnick RS, Haggerty DK (2005) Proton, helium, and electron spectra during the large solar particle events of October–November 2003. J Geophys Res Space Phys 110(A9). https://doi.org/10.1029/2005JA011038

Miyoshi Y, Sakaguchi K, Shiokawa K, Evans D, Albert J, Connors M, Jordanova V (2008) Precipitation of radiation belt electrons by EMIC waves, observed from ground and space. Geophys Res Lett 35(23). https://doi.org/10.1029/2008GL035727

Miyoshi Y, Oyama S, Saito S, Kurita S, Fujiwara H, Kataoka R, Ebihara Y, Kletzing C, Reeves G, Santolik O, Clilverd M, Rodger CJ, Turunen E, Tsuchiya F (2015) Energetic electron precipitation associated with pulsating aurora: EISCAT and Van Allen Probe observations. J Geophys Res Space Phys 120(4):2754–2766. https://doi.org/10.1002/2014JA020690

Miyoshi Y, et al (2018) Geospace exploration project ERG. Earth Planets Space 70:167. https://doi.org/10.1186/s40623-018-0862-0

Modzelewska R, Bazilevskaya GA, Boezio M, Koldashov SV, Krainev MB, Marcelli N, Mayorov AG, Mayorova MA, Munini R, Troitskaya IK, Yulbarisov RF, Luo X, Potgieter MS, Aslam OPM (2020) Study of the 27 day variations in GCR fluxes during 2007–2008 based on PAMELA and ARINA observations. Astrophys J 904(1):3. https://doi.org/10.3847/1538-4357/abbdac

Mohamed AMH, Emam I, Mohamed A (2018) Dosimetric validation of commissioning data validation of xio treatment planning system on a philips linear accelerator. J Cancer Sci Ther 10:36–40. https://doi.org/10.4172/1948-5956.1000514

Molchanov O, Rozhnoi A, Solovieva M, Akentieva O, Berthelier JJ, Parrot M, Lefeuvre F, Biagi PF, Castellana L, Hayakawa M (2006) Global diagnostics of the ionospheric perturbations related to the seismic activity using the VLF radio signals collected on the DEMETER satellite. Nat Hazards Earth Syst Sci 6(5):745–753. https://doi.org/10.5194/nhess-6-745-2006

Moses WW, et al (1987) Energetic electrons from Jupiter at 1 AU and their modulation by solar wind structures. Space Sci Rev 46:227–260

Munini R, Boezio M, Bruno A, Christian EC, de Nolfo GA, Di Felice V, Martucci M, Mergè M, Richardson IG, Ryan JM, Stochaj S, Adriani O, Barbarino GC, Bazilevskaya GA, Bellotti R, Bongi M, Bonvicini V, Bottai S, Cafagna F, Campana D, Carlson P, Casolino M, Castellini G, De Santis C, Galper AM, Karelin AV, Koldashov SV, Koldobskiy S, Krutkov SY, Kvashnin AN, Leonov A, Malakhov V, Marcelli L, Mayorov AG, Menn W, Mikhailov VV, Mocchiutti E, Monaco A, Mori N, Osteria G, Panico B, Papini P, Pearce M, Picozza P, Ricci M, Ricciarini SB, Simon M, Sparvoli R, Spillantini P, Stozhkov YI, Vacchi A, Vannuccini E, Vasilyev G, Voronov SA, Yurkin YT, Zampa G, Zampa N, Potgieter MS (2018) Evidence of energy and charge sign dependence of the recovery time for the 2006 December forbush event measured by the PAMELA experiment. Astrophys J 853(1):76. https://doi.org/10.3847/1538-4357/aaa0c8

Nakamura S, Omura Y, Kletzing C, Baker DN (2019) Rapid precipitation of relativistic electron by EMIC rising-tone emissions observed by the Van Allen Probes. J Geophys Res Space Phys 124(8):6701–6714. https://doi.org/10.1029/2019JA026772

Němek F, Santolík O, Parrot M, Berthelier JJ (2008) Spacecraft observations of electromagnetic perturbations connected with seismic activity. Geophys Res Lett 35(5). https://doi.org/10.1029/2007GL032517

NOAA-SWPC (2025) Products and data. https://www.swpc.noaa.gov/products/predicted-sunspot-number-and-radio-flux. Accessed 2025-05-26

Ogilvie KW, Desch MD, Farrugia CJ, Forsyth RJ, Aloise JA, et al (1995) Wind as part of the ISTP program: spacecraft, instruments, and measurement objectives. Space Sci Rev 71(1–4):1–14. https://doi.org/10.1007/BF00751326

Palma F, Martucci M, Neubüser C, Sotgiu A, Follega FM, Ubertini P, Bazzano A, Rodi JC, Ammendola R, Badoni D, Bartocci S, Battiston R, Beolè S, Bertello I, Burger WJ, Campana D, Cicone A, Cipollone P, Coli S, Conti L, Contin A, Cristoforetti M, D'Angelo G, De Angelis F, De Donato C, De Santis C, Diego P, Di Luca A, Fiorenza E, Gebbia G, Iuppa R, Lega A, Lolli M, Martino B, Masciantonio G, Mergè M, Mese M, Morbidini A, Nozzoli F, Nuccilli F, Oliva A, Osteria G, Palmonari F, Panico B, Papini E, Parmentier A, Perciballi S, Perfetto F, Perinelli A, Picozza P, Piersanti M, Pozzato M, Rebustini G, Recchiuti D, Ricci E, Ricci M, Ricciarini SB, Russi A, Sahnoun Z, Savino U, Scotti V, Shen X, Sparvoli R, Tofani S, Vertolli N, Vilona V, Vitale V, Zannoni U, Zeren Z, Zoffoli S, Zuccon P (2021a) Gamma-ray burst observations by the high-energy particle detector on board the China seismo-electromagnetic satellite between 2019 and 2021. Astrophys J 960(1):21. https://doi.org/10.3847/1538-4357/ad06ae

Palma F, Sotgiu A, Parmentier A, Martucci M, Piersanti M, Bartocci S, Battiston R, Burger WJ, Campana D, Carfora L, Castellini G, Conti L, Contin A, D'Angelo G, De Donato C, De Santis C, Follega FM, Iuppa R, Lazzizzera I, Marcelli N, Masciantonio G, Mergè M, Oliva A, Osteria G, Palmonari F, Panico B, Perfetto F, Picozza P, Pozzato M, Ricci E, Ricci M, Ricciarini SB, Sahnoun Z, Scotti V, Sparvoli R, Vitale V, Zoffoli S, Zuccon P (2021b) The August 2018 Geomagnetic Storm Observed by the High-Energy Particle Detector on Board the CSES-01 Satellite. Appl Sci 11(12):5680. https://doi.org/10.3390/app11125680

Papini E, Piersanti M, D'Angelo G, Cicone A, Bertello I, Parmentier A, Diego P, Ubertini P, Consolini G, Zhima Z (2023) Detecting the Auroral Oval through CSES-01 Electric Field Measurements in the Ionosphere. Remote Sens 15(6):1568. https://doi.org/10.3390/rs15061568

Parrot M (2002) The micro-satellite DEMETER. J Geodyn 33(4):535–541. https://doi.org/10.1016/S0264-3707(02)00014-5

Parrot M, Benoist D, Berthelier JJ, Błecki J, Chapuis Y, Colin F, Elie F, Fergeau P, Lagoutte D, Lefeuvre F, Legendre C, Lévêque M, Pinçon JL, Poirier B, Seran H-C, Zamora P (2006a) The magnetic field experiment IMSC and its data processing onboard DEMETER: scientific objectives, description and first results. Planet Space Sci 54(5):441–455. https://doi.org/10.1016/j.pss.2005.10.015

Parrot M, Berthelier JJ, Lebreton JP, Sauvaud JA, Santolik O, Blecki J (2006b) Examples of unusual ionospheric observations made by the DEMETER satellite over seismic regions. Phys Chem Earth 31(4–9):486–495. https://doi.org/10.1016/j.pce.2006.02.011

Picozza P, Galper AM, Castellini G, Adriani O, Altamura F, Ambriola M, Barbarino GC, Basili A, Bazilevskaja GA, Bencardino R, Boezio M, Bogomolov EA, Bonechi L, Bongi M, Bongiorno L, Bonvicini V, Cafagna F, Campana D, Carlson P, Casolino M, De Marzo C, De Pascale MP, De Rosa G, Fedele D, Hofverberg P, Koldashov SV, Krutkov SY, Kvashnin AN, Lund J, Lundquist J, Maksumov O, Malvezzi V, Marcelli L, Menn W, Mikhailov VV, Minori M, Misin S, Mocchiutti E, Morselli A, Nikonov NN, Orsi S, Osteria G, Papini P, Pearce M, Ricci M, Ricciarini SB, Runtso MF, Russo S, Simon M, Sparvoli R, Spillantini P, Stozhkov YI, Taddei E, Vacchi A, Vannuccini E, Voronov SA, Yurkin YT, Zampa G, Zampa N, Zverev VG (2007) PAMELA – a payload for antimatter matter exploration and light-nuclei astrophysics. Astropart Phys 27(4):296–315. https://doi.org/10.1016/j.astropartphys.2006.12.002

Picozza P, Battiston R, Ambrosi G, Bartocci S, Basara L, Burger WJ, Campana D, Carfora L, Casolino M, Castellini G, Cipollone P, Conti L, Contin A, De Donato C, De Santis C, Follega FM, Guandalini C, Ionica M, Iuppa R, Laurenti G, Lazzizzera I, Lolli M, Manea C, Marcelli L, Martucci M, Masciantonio G, Mergè M, Osteria G, Pacini L, Palma F, Palmonari F, Panico B, Parmentier A, Patrizii L, Perfetto F, Piersanti M, Pozzato M, Puel M, Rashevskaya I, Ricci E, Ricci M, Ricciarini S, Scotti V, Sotgiu A, Sparvoli R, Spataro B, Vitale V, Zuccon P, Zoffoli S (2019) Scientific goals and in-orbit performance of the high-energy particle detector on board the CSES. Astrophys J Suppl Ser 243(1):16. https://doi.org/10.3847/1538-4365/ab276c

Piersanti M, Del Moro D, Parmentier A, Martucci M, Palma F, Sotgiu A, Plainaki C, D'Angelo G, Berrilli F, Recchiuti D, Papini E, Giovannelli L, Napoletano G, Iuppa R, Diego P, Cicone A, Mergè M, De Donato C, De Santis C, Sparvoli R, Ubertini P, Battiston R, Picozza P (2022) On the magnetosphere-ionosphere coupling during the May 2021 geomagnetic storm. Space Weather 20(6):2021–003016. https://doi.org/10.1029/2021SW003016

Pinto M, Gonçalves P (2019) GUImesh: A tool to import STEP geometries into Geant4 via GDML. Comput Phys Commun 239:150–156. https://doi.org/10.1016/j.cpc.2019.01.024

Pulinets SA (1998) Seismic activity as a source of the ionospheric variability. Adv Space Res 22(6):903–906. https://doi.org/10.1016/S0273-1177(98)00121-5. IRI 1997 Symposium: New Developments in Ionospheric Modelling and Prediction

Rae IJ, Donovan EF, Mann IR, Fenrich FR, Watt CEJ, Milling DK, Lester M, Lavraud B, Wild JA, Singer HJ, Rème H, Balogh A (2005) Evolution and characteristics of global Pc5 ULF waves during a high solar wind speed interval. J Geophys Res Space Phys 110(A12). https://doi.org/10.1029/2005JA011007

Reigber C, Lühr H, Schwintzer P (eds) (2003) First CHAMP mission results for gravity, magnetic and atmospheric studies Springer, Berlin. https://doi.org/10.1007/978-3-540-38366-6

Rishbeth H (1988) Basic physics of the ionosphere: a tutorial review. J Inst Electron Radio Eng 58:207–223. https://doi.org/10.1049/jiere.1988.0060

Rogers F, Aramaki T, Boezio M, Boggs SE, Bonvicini V, Bridges G, Campana D, Craig WW, von Doetinchem P, Everson E, Fabris L, Feldman S, Fuke H, Gahbauer F, Gerrity C, Hailey CJ, Hayashi T, Kawachi A, Kozai M, Lenni A, Lowell A, Manghisoni M, Marcelli N, Mochizuki B, Mognet SAI, Munakata K, Munini R, Nakagami Y, Olson J, Ong RA, Osteria G, Perez KM, Quinn S, Re V, Riceputi E, Roach B, Ryan J, Saffold N, Scotti V, Shimizu Y, Sparvoli R, Stoessl A, Tiberio A, Vannuccini E, Wada T, Xiao M, Yamatani M, Yee K, Yoshida A, Yoshida T, Zampa G, Zeng J, Zweerink J (2023) Sensitivity of the GAPS experiment to low-energy cosmic-ray antiprotons. Astropart Phys 145:102791. https://doi.org/10.1016/j.astropartphys.2022.102791

Rossi S (2011) The status of CNAO. Eur Phys J Plus 126(8):78. https://doi.org/10.1140/epjp/i2011-11078-8

Rouillard AP, Sheeley NR, Cooper TJ, Davies JA, Lavraud B, Kilpua EKJ, Skoug RM, Steinberg JT, Szabo A, Opitz A, Sauvaud J-A (2011) The solar origin of small interplanetary transients. Astrophys J 734(1):7. https://doi.org/10.1088/0004-637X/734/1/7

Sarkar S, Gwal AK, Parrot M (2007) Ionospheric variations observed by the DEMETER satellite in the mid-latitude region during strong earthquakes. J Atmos Sol-Terr Phys 69(13):1524–1540. https://doi.org/10.1016/j.jastp.2007.06.006

Sgrigna V, Carota L, Conti L, Corsi M, Galper AM, Koldashov SV, Murashov AM, Picozza P, Scrimaglio R, Stagni L (2005) Correlations between earthquakes and anomalous particle bursts from SAMPEX/PET satellite observations. J Atmos Sol-Terr Phys 67(15):1448–1462. https://doi.org/10.1016/j.jastp.2005.07.008

Shen X, Zhang X, Yuan S, Wang L, Cao J, Huang J, Zhu X, Piergiorgio P, Dai J (2018) The state-of-the-art of the China Seismo-Electromagnetic Satellite mission. Sci China, Technol Sci 61(5):634–642. https://doi.org/10.1007/s11431-018-9242-0

Shprits YY, Thorne RM (2004) Time dependent radial diffusion modeling of relativistic electrons with realistic loss rates. Geophys Res Lett 31(8):08805. https://doi.org/10.1029/2004GL019591

Sibeck DG, Angelopoulos V (2008) THEMIS science objectives and mission phases. Space Sci Rev 141:1–25. https://doi.org/10.1007/s11214-008-9393-5

Siruk SA, Kuznetsov AV, Mayorov AG, Yulbarisov RF (2024) Analysis of the spectrum of 27-day GCR variations in 2015–2016. Adv Space Res 74(4):1978–1992. https://doi.org/10.1016/j.asr.2024.05.050

Sotgiu A, De Donato C, Fornaro C, Tassa S, Scannavini M, Iannaccio D, Ambrosi G, Bartocci S, Basara L, Battiston R, Burger WJ, Campana D, Carfora L, Castellini G, Cipollone P, Conti L, Contin A, De Persio F, De Santis C, Follega FM, Guandalini C, Ionica M, Iuppa R, Laurenti G, Lazzizzera I, Lolli M, Manea C, Martucci M, Masciantonio G, Mergè M, Osteria G, Pacini L, Palma F, Palmonari F, Panico B, Parmentier A, Perfetto F, Picozza P, Piersanti M, Pozzato M, Puel M, Rashevskaya I, Ricci E, Ricci M, Ricciarini SB, Scotti V, Sparvoli R, Spataro B, Vitale V, Zoffoli S, Zuccon P (2020) Control and data acquisition software of the High-Energy Particle Detector on board the China Seismo-Electromagnetic Satellite space mission. Softw Pract Exp, 1–22. https://doi.org/10.1002/spe.2947

Spence HE, Reeves GD, Baker DN, et al (2013) Science goals and overview of the Radiation Belt Storm Probes (RBSP) Energetic Particle, Composition, and Thermal Plasma (ECT) suite on NASA's Van Allen Probes mission. Space Sci Rev 179(1–4):311–336. https://doi.org/10.1007/s11214-013-0007-5

Stone EC, Frandsen AM, Mewaldt RA, Christian ER, Margolies D, Ormes JF, Snow F (1998) The Advanced Composition Explorer. Space Sci Rev 86(1):1–22. https://doi.org/10.1023/A:1005082526237

Stone EC, Cummings AC, McDonald FB, Heikkila BC, Lal N, Webber WR (2013) Voyager 1 observes low-energy galactic cosmic rays in a region depleted of heliospheric ions. Science 341(6142):150–153. https://doi.org/10.1126/science.1236408

Stone EC, Cummings AC, Heikkila BC, Lal N (2019) Cosmic ray measurements from Voyager 2 as it crossed into interstellar space. Nat Astron 3(11):1013–1018. https://doi.org/10.1038/s41550-019-0928-3

Strauss RD, Potgieter MS, Büsching I, Kopp A (2011) Modeling the modulation of galactic and Jovian electrons by stochastic processes. Astrophys J 735(2):83. https://doi.org/10.1088/0004-637X/735/2/83

Summers D, Thorne RM (2003) Relativistic electron pitch-angle scattering by electromagnetic ion cyclotron waves during geomagnetic storm. J Geophys Res Space Phys 108(A4). https://doi.org/10.1029/2002JA009489

Summers D, Ni B, Meredith NP (2007) Timescales for radiation belt electron acceleration and loss due to resonant wave-particle interactions: 2. Evaluation for VLF chorus, ELF hiss, and electromagnetic ion cyclotron waves. J Geophys Res Space Phys 112(4). https://doi.org/10.1029/2006JA011993

Thorne RM (2010) Radiation belt dynamics: the importance of wave-particle interactions. Geophys Res Lett 37(22). https://doi.org/10.1029/2010GL044990

Titheridge JE (1995) Winds in the ionosphere—a review. J Atmos Terr Phys 57(14):1681–1714. https://doi.org/10.1016/0021-9169(95)00091-F. The Second South Pacific Step Workshop, Newcastle, Australia

Tommasino F, Rovituso M, Fabiano S, Piffer S, Manea C, Lorentini S, Lanzone S, Wang Z, Pasini M, Burger WJ, La Tessa C, Scifoni E, Schwarz M, Durante M (2017) Proton beam characterization in the experimental room of the Trento Proton Therapy facility. Nucl Instrum Methods Phys Res, Sect A, Accel Spectrom Detect Assoc Equip 869:15–20. https://doi.org/10.1016/j.nima.2017.06.017

Tsurutani BT, Verkhoglyadova OP, Mannucci AJ, Lakhina GS, Li G, Zank GP (2009) A brief review of "solar flare effects" on the ionosphere. Radio Sci 44:RS0A17. https://doi.org/10.1029/2008RS004029

Usoskin IG (2023) A history of solar activity over millennia. Living Rev Sol Phys 20:2. https://doi.org/10.1007/s41116-023-00036-z

Webber WR, et al (1973) Measurements of the primary cosmic-ray electron spectrum from balloon flights (1965–1972). Int Cosm Ray Conf 2:760

Yan R, Zhima Z, Xiong C, Shen X, Huang J, Guan Y, Zhu X, Liu C (2020) Comparison of Electron Density and Temperature from the CSES Satellite with Other Space-Borne and Ground-Based Observations. J Geophys Res Space Phys 125(10). https://doi.org/10.1029/2019JA027747

Yang Y-Y, Zhima Z-R, Shen X-H, Chu W, Huang J-P, Wang Q, Yan R, Xu S, Lu H-X, Liu D-P (2020) The First Intense Geomagnetic Storm Event Recorded by the China Seismo-Electromagnetic Satellite. Space Weather 18(1). https://doi.org/10.1029/2019SW002243

Zhang J, Temmer M, Gopalswamy N, Malandraki O, Nitta NV, Patsourakos S, Shen F, Vršnak B, Wang Y, Webb D, Desai MI, Dissauer K, Dresing N, Dumbović M, Feng X, Heinemann SG, Laurenza M, Lugaz N, Zhuang B (2021) Earth-affecting solar transients: a review of progresses in solar cycle 24. Prog Earth Planet Sci 8(1):56. https://doi.org/10.1186/s40645-021-00426-7

Zhao S, Zhou C, Shen X, Zhima Z (2019) Investigation of VLF transmitter signals in the ionosphere by ZH-1 observations and full-wave simulation. J Geophys Res Space Phys 124(6):4697–4709. https://doi.org/10.1029/2019JA026593

Zhima Z, Huang J, Shen X, Xia Z, Chen L, Piersanti M, Yang Y, Wang Q, Zeng L, Lei J, Chu W, Yan R, Zhao S, Hu Y, Guo F (2020) Simultaneous Observations of ELF/VLF Rising-Tone Quasiperiodic Waves and Energetic Electron Precipitations in the High-Latitude Upper Ionosphere. J Geophys Res Space Phys 125(5). https://doi.org/10.1029/2019JA027574

Zhima Z, Hu Y, Shen X, Chu W, Piersanti M, Parmentier A, Zhang Z, Wang Q, Huang J, Zhao S, Yang Y, Yang D, Sun X, Tan Q, Zhou N, Guo F (2021) Storm-time features of the ionospheric elf/vlf waves and energetic electron fluxes revealed by the China seismo-electromagnetic satellite. Appl Sci 11(6). https://doi.org/10.3390/app11062617

Zhu C-R, Yuan Q, Wei D-M (2018) Studies on cosmic-ray nuclei with Voyager, ACE, and AMS-02. I. Local interstellar spectra and solar modulation. Astrophys J 863(2):119. https://doi.org/10.3847/1538-4357/aacff9

Authors and Affiliations

Simona Bartocci[1] · Roberto Battiston[2,3] · Stefania Beolè[4,5] · Franco Benotto[5] · Piero Cipollone[6] · Silvia Coli[5] · Andrea Contin[7,8] · Marco Cristoforetti[9,3] · Cinzia De Donato[6] · Cristian De Santis[6] · Andrea Di Luca[9,3] · Flori Dumitrache[5] · Francesco Maria Follega[2,3] · Simone Garrafa Botta[5] · Giuseppe Gebbia[3] · Roberto Iuppa[2,3] · Alessandro Lega[9,3] · Mauro Lolli[8] · Matteo Martucci[6] · Giuseppe Masciantonio[6] · Matteo Mergè[10] · Marco Mese[11,12] · Riccardo Nicolaidis[2,3] · Francesco Nozzoli[3] · Alberto Oliva[8] · Giuseppe Osteria[12] · Francesco Palma[6] · Federico Palmonari[7,8] · Beatrice Panico[11,12] · Stefania Perciballi[4,5] · Francesco Perfetto[12] · Alessio Perinelli[2,3] · Piergiorgio Picozza[13,6] · Michele Pozzato[8] · Ester Ricci[2,3] · Leonardo Ricci[2,3] · Marco Ricci[6,14] · Sergio Bruno Ricciarini[15] · Zouleikha Sahnoun[7,8] · Umberto Savino[4,5] · Valentina Scotti[11,12] · Enrico Serra[3] · Matteo Sorbara[13,6] · Alessandro Sotgiu[6] · Roberta Sparvoli[13,6] · Pietro Ubertini[16] · Veronica Vilona[9,3] · Simona Zoffoli[10] · Paolo Zuccon[2,3]

✉ C. De Santis
cristian.desantis@roma2.infn.it

✉ R. Iuppa
roberto.iuppa@unitn.it

1 INFN – AC, V. E. Fermi 54, Frascati (RM), 00044, Italy

2 University of Trento, V. Sommarive 14, Povo (TN), 38123, Italy

3 INFN – TIFPA, V. Sommarive 14, Povo (TN), 38123, Italy

4 University of Turin, V. P. Giuria 1, Turin, 10125, Italy

5 INFN – Sezione di Torino, V. P. Giuria 1, Turin, 10125, Italy

6 INFN – Sezione di Roma Tor Vergata, V. della Ricerca Scientifica 1, Rome, 00133, Italy

7 University of Bologna, V.le Berti Pichat 6, Bologna, 40127, Italy

8 INFN – Sezione di Bologna, V.le Berti Pichat 6, Bologna, 40127, Italy

9 Fondazione Bruno Kessler, V. Sommarive 18, Povo (TN), 38123, Italy

10 Italian Space Agency, V. del Politecnico, Rome, 00133, Italy

11 University of Napoli "Federico II", V. Cintia, Napoli, 80126, Italy

12 INFN – Sezione di Napoli, V. Cintia, Napoli, 80126, Italy

13 University of Roma Tor Vergata, V. della Ricerca Scientifica 1, Rome, 00133, Italy

14 INFN – LNF, V. E. Fermi 54, Frascati (RM), 00044, Italy

15 IFAC-CNR, V. Madonna del Piano 10, Sesto Fiorentino (FI), 50019, Italy

16 INAF-IAPS, V. Fosso del Cavaliere 100, Rome, 00133, Italy